Biogeosciences, 13, 841–863, 2016
www.biogeosciences.net/13/841/2016/
doi:10.5194/bg-13-841-2016

Biogeosciences Open Access EGU

The impact of sedimentary alkalinity release on the water column CO_2 system in the North Sea

H. Brenner[1], **U. Braeckman**[2], **M. Le Guitton**[1], **and F. J. R. Meysman**[1,3]

[1]Department of Ecosystem Studies, Royal Netherlands Institute for Sea Research (NIOZ), Korringaweg 7, 4401 NT Yerseke, the Netherlands
[2]Marine Biology Research Group, Ghent University, Krijgslaan 281 S8, 9000 Ghent, Belgium
[3]Department of Analytical, Environmental and Geochemistry, Free University of Brussels (VUB), Pleinlaan 2, 1050 Brussels, Belgium

Correspondence to: H. Brenner (heiko.brenner@nioz.nl)

Received: 9 July 2015 – Published in Biogeosciences Discuss.: 7 August 2015
Revised: 15 January 2016 – Accepted: 15 January 2016 – Published: 12 February 2016

Abstract. It has been previously proposed that alkalinity release from sediments can play an important role in the carbonate dynamics on continental shelves, lowering the pCO_2 of seawater and hence increasing the CO_2 uptake from the atmosphere. To test this hypothesis, sedimentary alkalinity generation was quantified within cohesive and permeable sediments across the North Sea during two cruises in September 2011 (basin-wide) and June 2012 (Dutch coastal zone). Benthic fluxes of oxygen (O_2), alkalinity (A_T) and dissolved inorganic carbon (DIC) were determined using shipboard closed sediment incubations. Our results show that sediments can form an important source of alkalinity for the overlying water, particularly in the shallow southern North Sea, where high A_T and DIC fluxes were recorded in nearshore sediments of the Belgian, Dutch and German coastal zone. In contrast, fluxes of A_T and DIC are substantially lower in the deeper, seasonally stratified, northern part of the North Sea. Based on the data collected, we performed a model analysis to constrain the main pathways of alkalinity generation in the sediment, and to quantify how sedimentary alkalinity drives atmospheric CO_2 uptake in the southern North Sea. Overall, our results show that sedimentary alkalinity generation should be regarded as a key component in the CO_2 dynamics of shallow coastal systems.

1 Introduction

Coastal seas play a crucial role in the global carbon cycle by connecting the terrestrial, oceanic and atmospheric reservoirs (Regnier et al., 2013). Although continental shelves cover only 7 % of the global ocean surface, they account for up to 30 % of the oceanic primary production (Gattuso et al., 1998) and between 10 and 25 % of the present-day oceanic CO_2 uptake (Regnier et al., 2013; Bauer et al., 2013). In general, most open shelves in the temperate and high-latitude regions are undersaturated with respect to atmospheric CO_2, while the low-latitude shelves tend to be supersaturated (Cai et al., 2006; Chen and Borges, 2009). However, this rule is far from absolute. Although temperate coastal areas generally act as a CO_2 sink, considerable variability has been observed in the CO_2 uptake within and between systems, which may be explained by a dominance of different drivers of CO_2 uptake. High nutrient inputs from land fuel intense primary production and hence stimulate atmospheric CO_2 uptake, while respiration of organic matter exported from terrestrial ecosystems stimulates the release of CO_2 in coastal areas (Bozec et al., 2006; Jönsson et al., 2011; Schiettecatte et al., 2007). In addition to these biological sinks and sources, the effect of temperature on the CO_2 solubility controls the magnitude and direction of the CO_2 exchange between coastal waters and the atmosphere (Kitidis et al., 2012; Borges and Frankignoulle, 2003). Therefore the question remains which particular drivers are governing the CO_2 dynamics in a given coastal system (Borges and Frankignoulle, 2003).

In addition to water column processes, sediments have also been suggested to play a role in coastal CO_2 uptake, as the shallowness of coastal seas permits a close interaction between the sediment, the water body, and the atmosphere. Coastal water bodies are characterized by either a permanently or seasonally mixed water column, which hence establishes a direct link between the sediment and the atmosphere, acting on a timescale of days to months. In contrast, in the open ocean, the sediment and the atmosphere can only interact over much longer timescales (≈ 1000 years of global oceanic circulation). However, the extent to which sediment geochemistry plays a role in the overall CO_2 uptake of coastal systems remains largely unresolved.

It has been proposed that alkalinity generation caused by anaerobic organic matter degradation in shallow coastal sediments can increase the CO_2 buffer capacity of coastal waters and therefore increase atmospheric CO_2 uptake. When coining this hypothesis, Thomas et al. (2009) estimated that alkalinity generation in Wadden Sea sediments could be responsible for 20–25 % of the total CO_2 uptake of the entire North Sea. However, Moore et al. (2011) estimated much smaller A_T fluxes between the Wadden Sea and the North Sea based on activity measurements of radium isotopes in surface water. While the strength of the A_T flux between the Wadden Sea and the North Sea remains under debate, the Wadden Sea has been identified as a source of A_T for the North Sea (Brasse et al., 1999; Thomas et al., 2009; Provoost et al., 2010; Moore et al., 2011). However, it remains an open question whether this A_T export from the Wadden Sea drives any CO_2 uptake in the North Sea (maybe the A_T-induced CO_2 uptake has already taken place in the Wadden Sea), and also, how important the sediments of the North Sea proper are in driving CO_2 uptake in the North Sea. In the East China Sea it was already suggested by Chen and Wang (1999) that alkalinity generation due to anaerobic degradation processes in sediments adds considerably to the total alkalinity budget in this area. Furthermore, Chen (2002) proposed that shelf-generated alkalinity release from benthic anaerobic processes could be almost as important as alkalinity generated by dissolution of carbonates in the open ocean. Finally, based on modeled nitrogen and carbon budgets for the northwestern North Atlantic continental shelf, Fennel (2010) suggested that shelf sediments must be an important source of alkalinity. By contrast, Hu and Cai (2011a) estimated a much smaller mean alkalinity flux from global coastal sediments based on the upscaling of local denitrification and sulfate reduction rates. They concluded that sedimentary alkalinity fluxes are generally too low to significantly affect the alkalinity budget of the global ocean, but also stated that sedimentary anaerobic processes could be important on regional scales as an alkalinity release mechanism. From these results, it is clear that presently, there is uncertainty as to what extent coastal sediments are an important source of alkalinity to the coastal ocean and whether this benthic alkalinity release then induces any significant CO_2 uptake in the coastal ocean.

In this study, the objective was to quantify sedimentary alkalinity generation within various sediment types in the North Sea. During two cruises, samples were collected in September 2011 (basin-wide) and June 2012 (Dutch coastal zone). Benthic fluxes of alkalinity, dissolved inorganic carbon and oxygen were determined using closed sediment incubations and microsensor profiling. Subsequently, we used this data set in a model analysis to constrain the sources of the sedimentary alkalinity release in the shallow southern North Sea. This way, we were able to construct an alkalinity budget for both sediment and water column, and based on this budget, we then could estimate the net CO_2 uptake from the atmosphere associated with the sedimentary alkalinity release.

2 Materials and methods

2.1 North Sea system

In this paper we divide the North Sea into three different hydrogeographical zones: the southern North Sea (SNS), the northern North Sea (NNS), and the combination of the Skagerrak and the Norwegian Trench (SKNT). The SNS (surface area: 279.2 km^2) encompasses the Southern Bight (between Belgium–Netherlands and the UK), the shallow Wadden Sea (running along the Dutch and German coast up to Esbjerg in Denmark), the German Bight, and the central part of the North Sea (Fig. 1). The major difference between the SNS and the NNS is the stratification regime. Whereas the shallow SNS has a fully mixed water column throughout the year, the NNS is thermally stratified in summer but fully mixed during winter, due to strong wind forcing and surface cooling (Elliott et al., 1991). As the operational border between the SNS and NNS, we use the absence/presence of stratification as observed in September 2011. Thus, all non-stratified stations are classified as SNS, while all stratified stations belong to either the NNS or the SKNT. The third hydrogeographical zone is the Skagerrak and the Norwegian Trench (SKNT), which forms one of the major sediment depositional areas of the North Sea (de Haas and van Weering, 1997). The Skagerrak is part of the transition area that connects the North Sea with the Baltic Sea. It is a rather small strait (200 by 100 km) between the southeastern coast of Norway, the southwestern coast of Sweden, and the Jutland Peninsula of Denmark. The average depth of the Skagerrak is about 210 m. The Skagerrak is strongly stratified in summer, but also features a weak stratification in winter driven by Baltic freshwater inputs (Gustafsson and Stigebrandt, 1996; Rodhe, 1987). The Skagerrak is connected to the Norwegian Sea through the Norwegian Trench, with a sill depth of 270 m. The Norwegian Trench itself is a deep sedimentary basin (250–700 m) that reaches from the Oslofjord in the southeast to the Stad Peninsula in the upper northwest (Rodhe, 1996). Like the Skagerrak, the Norwegian Trench

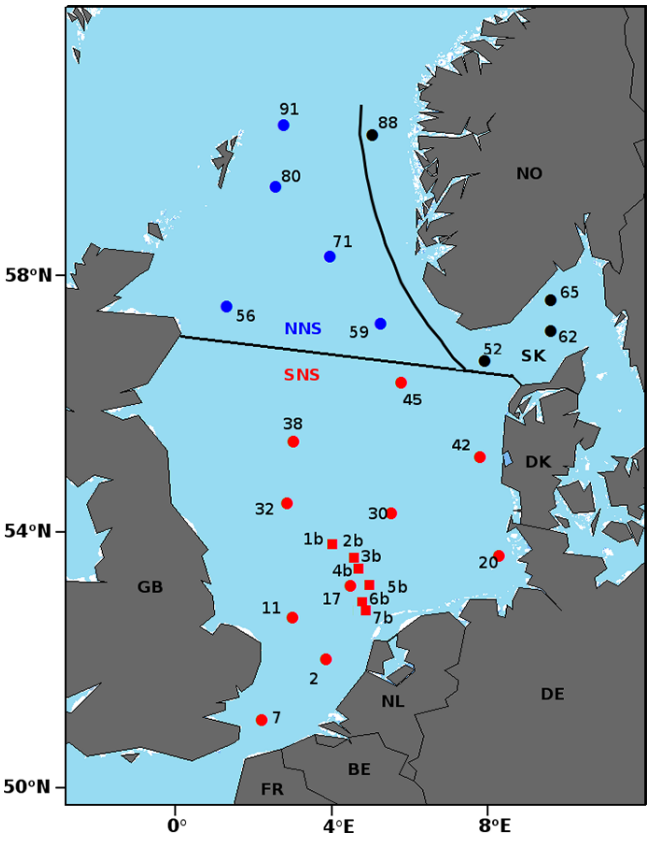

Figure 1. Map of sampled stations. Red symbols: southern North Sea; black symbols: Skagerrak; blue symbols: northern North Sea; circles: sampled in September 2011; squares: sampled in June 2012. Border of the Skagerrak as defined by the International Hydrographic Organization; the border between SNS and NNS roughly represents the 100 m depth isoline.

is characterized by haline stratified water masses (Reid and Edwards, 2001).

The water transport in the NNS is dominated by the large open boundary with the North Atlantic. Water entering in the west through the Shetland Channel and the Faire Island Channel turns eastwards and leaves the North Sea via the Norwegian Trench in the east. The residence time of this water is about 1 year. Generally, water entering the NNS does not influence the SNS, as just 5 % of the North Atlantic water entering the northern boundary reaches the SNS (Lenhart and Pohlmann, 1997). The water transport in the SNS is mainly determined by inflow from the Atlantic Ocean through the channel, which mixes with low-salinity water coming from rivers and moves along the eastern coastlines towards the northeast. Baltic Sea water entering through the Kattegat and coastal run-off are important in maintaining the Norwegian Coastal Current that initiates in the Skagerrak. This northwards-directed current is the only net outflow of the North Sea and thus balances all incoming water inputs as described above. Additionally, the shallow SNS is influenced by strong tidally induced currents and mixing (Dauwe, 1999). The tides in the SNS are diurnal, whereas maximum surface currents at spring tide occur in the western and southern parts of the SNS. More to the north and into the German Bight, the tidal current velocities decrease (Van der Molen, 2002).

The seafloor of the North Sea predominantly consists of permeable sediments. Medium and fine sand is the main sediment type and occupies the largest part of the North Sea basin. Coarse sand is found at confined locations throughout the entire North Sea basin, with larger areas of coarse-grained sediments present along the English coast and in front of the German and Danish coasts. Mud and sandy mud are mainly found in the deep trenches along the Norwegian coast, off the coast of Scotland, in particular locations along the Belgian coast, in smaller areas north and east of the German Bight, and near Helgoland in the German Bight (Lüders, 1955; Schlüter and Jerosch, 2009; Hebbeln et al., 2003; Braeckman et al., 2014).

2.2 Sediment sampling

During a cruise onboard R/V *Pelagia* in September 2011, we sampled a total of 19 stations across the whole North Sea basin (Table 1). On a second cruise in June 2012, we sampled seven stations along a transect perpendicular to the Dutch coast from the Wadden island of Terschelling up to the Oyster Ground in the central North Sea (1b–7b in Fig. 1). Sediment cores were collected at each site using a Reineck box corer. Polymethyl methacrylate (PMMA) core barrels (19 cm inner diameter) were subsequently inserted into the sediment of the box core to a depth of 10 to 15 cm enclosing 15 to 20 cm of overlying water. The cores were excavated from the box core, closed off with a lid at the bottom, and immediately transferred to a water-filled reservoir in a thermo-controlled container that was kept at in situ bottom water temperature. These sediment cores were subsequently used for closed core flux incubations as described below.

During the September 2011 cruise, small sediment cores were retrieved for solid-phase analysis and microsensor profiling, and these were taken from the same box core as the flux cores. For solid-phase analysis, acrylic core barrels (5 cm i.d.) were inserted into the sediment of the box core. The upper 10 cm of each core were sliced into 1 cm intervals and sediment samples were analyzed for porosity and grain size distribution. Porosity was determined by weight loss after freeze-drying, accounting for salt precipitation in the saline pore water. Grain size distribution was determined using a Malvern Mastersizer 2000 particle analyzer.

For O_2 and pH microsensor profiling, acrylic core liners (3 cm i.d.) were inserted into the sediment of the box core, and afterwards, the sediment was brought level to the rim of the core liner. Cores were subsequently placed in an aquarium containing bottom water at in situ temperature, which was constantly bubbled with ambient air, to ensure constant

Table 1. Sampled stations from both cruises in 2011 and 2012 with coordinates and maximum water depth, as well as with sediment characteristics and bottom water characteristics as measured by the CTD.

Station	Region	Latitude	Longitude	Water depth	Temperature Bottom water	Salinity Bottom water	Oxygen Bottom water	Porosity	Median Grain size	Sediment classification
2011	North Sea basin-wide			(m)	(°C)	(PSU)	(µmol kg^{-1})	(vol vol^{-1})	(µm)	(Wentworth)
2	SNS	52.60000	3.50117	29.84	17.11	35.06	153.80	0.32	292	Medium sand
7	SNS	51.52533	1.96633	40.66	17.41	34.94	153.49	–	499	Medium sand
11	SNS	53.19983	2.50083	30.53	16.33	34.51	157.290	0.32	287	Medium sand
17	SNS	53.80033	4.00050	29.95	17.03	34.14	150.84	0.35	237	Fine sand
20	SNS	54.40033	8.10050	18.23	17.16	29.35	151.10	0.32	209	Fine sand
30	SNS	55.00000	4.99950	39.40	15.29	34.76	155.67	0.37	150	Fine sand
32	SNS	55.00000	1.99983	22.99	14.25	34.63	154.34	0.32	215	Fine sand
38	NNS	1.99983	1.99983	81.09	7.32	34.45	140.10	0.42	138	Fine sand
42	SNS	56.00167	7.50033	20.19	16.29	33.87	154.17	0.31	219	Fine sand
45	NNS	57.00000	5.25100	53.96	7.02	35.01	146.19	0.33	287	Medium sand
52	SKNT	57.50050	7.50150	209.65	6.18	35.18	165.70	0.63	62	Coarse silt
56	NNS	58.00000	−0.49933	109.03	9.29	35.37	143.73	0.46	119	Fine sand
59	NNS	58.00050	4.25100	95.23	7.66	35.21	151.43	0.31	314	Medium sand
62	SKNT	58.00000	9.50083	304.24	6.03	35.15	169.51	0.64	36	Coarse silt
65	SKNT	58.49983	9.49983	539.12	6.02	35.18	172.03	0.74	28	Medium silt
71	NNS	59.00033	2.50000	115.11	6.87	35.27	148.17	0.40	149	Fine sand
80	NNS	60.00017	0.50000	116.46	8.90	35.39	150.42	0.35	283	Medium sand
88	SKNT	61.00000	3.49950	350.27	6.29	35.39	150.42	0.35	21	Medium silt
91	NNS	60.99950	0.50033	141.16	7.60	35.33	146.49	0.44	269	Medium sand
2012	Dutch coastal transect									
1b	SNS	54.43190	3.40820	43.92	8.68	34.64	267.63			
2b	SNS	54.24760	4.02550	44.65	9.51	34.73	260.38			
3b	SNS	54.08090	4.20060	47.58	11.21	34.67	253.80			
4b	SNS	53.55040	4.36280	35.55	12.21	34.74	264.95			
5b	SNS	53.82750	4.52470	41.00						
6b	SNS	53.41270	4.28640	36.33	12.43	34.55	272.63			
7b	SNS	53.42550	4.48820	36.66						

water flow over the sediment. Bottom water was retrieved by casts with 25 L Niskin bottles (Ocean Test Equipment, Fort Lauderdale, USA) retrieving water at approximately 1 m above the sediment surface. A conductivity, temperature, depth (CTD) was mounted on a standard rosette frame together with 24 Niskin bottles. The CTD was equipped with a SBE3+ thermometer, a SBE4 conductivity meter and a SBE43 dissolved oxygen sensor (Seabird, USA).

2.3 Solute flux measurements

Flux chamber incubations are potentially susceptible to various methodological artifacts resulting from sediment enclosure, which relate to the sensitivity of benthic fluxes to changes in ambient hydrodynamics and altered benthic faunal activity (Santschi et al., 1991; Tengberg et al., 2005; Lehrter et al., 2011). In permeable sediments, fluxes are particularly susceptible to the imposed stirring regime and the associated local pressure gradients that are generated in the flux chamber, which drive the advective pore-water exchange between sediment and overlying water (Huettel and Gust, 1992; Janssen et al., 2005). The flux chamber type employed here was based on the design in Huettel and Gust (1992), which was specifically developed for flux studies in permeable sediments. The sediment cores retrieved were closed off with a PMMA top lid that was equipped with a large central stirring disc (diameter: 14 cm). The rotation of the disc mixes the overlying water and establishes a specific radial pressure gradient, which drives pore-water exchange in the chamber. A major challenge for flux chamber studies in permeable sediments is the selection of the appropriate stirring regime. Without knowledge of the local in situ hydrodynamics, it is impossible to predict a priori which stirring regime is appropriate for a given site. Here we used two different stirring rates at each station (40 and 80 rpm) to mimic a range of interfacial pressure gradients and solute exchange conditions (Huettel and Gust, 1992; Janssen et al., 2005; Rao et al., 2012). By taking this approach, we are able to discern how sensitive the fluxes at each station are to advective exchange, and thus we get an idea of the uncertainty in our flux estimates for the permeable sites that we visited.

Prior to the start of the flux measurements, the overlying water in each core was replaced with ambient bottom water to ensure that the chemical composition of the overlying water closely resembled in situ conditions. Each set of flux measurements began by securing gas-tight lids equipped with O-ring seals on each core. Core lids contained two sampling ports on opposite sides for subsampling during the incubation, and these ports were carefully purged with bottom water prior to the start of each incubation to remove any air bubbles trapped. Fiber-optical oxygen sensors (FireSting OXF1100) were inserted into a third opening in the top lid. The chambers were closely inspected to ensure that no gas bubbles remained inside the chamber. Two or three replicate chamber incubations were made per station.

The temporal evolution of the oxygen concentration in the overlying water of the flux chambers was continuously monitored using oxygen optodes at a sample interval of 1 min. Optodes were pre-calibrated on the same day using a two-point calibration with ambient seawater at 0 % (saturated with sodium sulfite) and 100 % O_2 saturation (bubbled with air). Optode results were verified with measurements of the O_2 concentration by Winkler titration in discrete water samples before and after incubation (Grasshoff et al., 2009).

A water subsample ($\sim$ 50 mL) was withdrawn from the chambers at 4–6 h intervals for solute analysis as described below. When a water sample was extracted via one sampling port, an equal amount of ambient bottom water entered through the replacement tube connected to the other sampling port. Samples were collected in plastic syringes for alkalinity (A_T) and in glass syringes for dissolved inorganic carbon (DIC) analysis. Water samples for A_T ($\sim$ 10 mL) were filtered (0.45 µm Millex-HA syringe filter) and stored in the dark at 4 °C. DIC water samples ($\sim$ 12 mL) were not filtered, but were poisoned with 10 µL $HgCl_2$ and stored submerged at 4 °C in a fridge.

The total oxygen uptake (TOU) rate and the flux of DIC and A_T were determined from a linear regression of overlying water concentrations versus incubation time (Eq. 1).

$$J = \frac{V_{ow}}{A} \frac{dC_{ow}}{dt} \quad (1)$$

In this, V_{ow} is the volume of overlying water, A is the surface area of sediment, and C_{ow} is the concentration in overlying water. At the end of the incubation, the top lid was removed, the height of the overlying water ($H = V_{ow}/A$) was measured at four points along the side of the core using a ruler, and the mean height was calculated. Glud (2008) suggested that an oxygen decrease by more than 10–15 % from the initial conditions can already stimulate processes that cause a nonlinear decrease in oxygen concentrations, which also might affect other solute fluxes across the sediment–water interface. Here we found that the linear regressions used to calculate the oxygen uptake were insensitive to an oxygen decrease of 30 % or more (for examples, see Fig. 3).

2.4 Analytical methods

Total A_T was determined via an open-cell titration procedure, using a Metrohm Titrando 888 system with a combined Metrohm glass electrode (Unitrode) following the SOP3a procedure as described in Dickson et al. (2007). Samples (10 mL) were placed in a temperature-regulated open cell (25 °C) and titrated with a solution of hydrochloric acid (0.1 N) in a two-stage process. First the sample (10 mL) was acidified to a pH close to 3.5 and then titrated in small steps down to a pH of 3.0. Subsequently, A_T was calculated using a nonlinear regression approach based on SOP3a from Dickson et al. (2007). Two replicate measurements were carried out for each sample analyzed. Titrations ($n = 10$) of certi-

fied reference materials (CRM batch 116 provided by A.G. Dickson) were on average within 4 µmol kg^{-1} of the nominal value, with a precision of 5 µmol kg^{-1}.

DIC was determined using an AS-C3 DIC analyzer (Apollo SciTEch, USA), in which the sample (0.8 mL) was acidified and the released CO_2 was detected using a solid state infra-red CO_2 detector (LI-7000, LI-COR Biosciences, USA). Two replicate measurements were carried out for each sample analyzed. Quality assurance of the DIC analysis was also based on CRM (batch 116; accuracy and precision: 3 µmol kg^{-1}).

2.5 O_2 and pH microprofiling

Microsensor profiling was performed using commercial Clark-type O_2 and potentiometric pH microsensors operated with a motorized micromanipulator (Unisense A.S., Denmark). To minimize the error by ship movement, the microprofiling setup was placed in the center, the most stable location of the ship. Under strong wind conditions, microprofiling was not performed, in order to prevent sensor damage. Vertical depth profiles of O_2 were recorded using an electrode with a tip size of 100 at 250 µm steps, beginning at 2 mm above the sediment–water interface until either anoxia or 20 mm depth. The O_2 microsensors were calibrated with a two-point calibration made in air-saturated seawater (100 % saturation) and at depth in anoxic sediment (0 % saturation). Depth profiles of pH were measured using microsensors with a tip size of 200 µm in 1 mm steps, beginning 4 mm above the sediment surface until 35 mm depth. Measurements were always started within 1 h after sampling. The pH microsensors were calibrated using NBS buffers (pH 4 and 7) and TRIS buffers (DelValls and Dickson, 1998), and the pH is reported on the total scale.

The diffusive oxygen uptake (DOU) of the sediment was calculated from the O_2 depth profiles as

$$\mathrm{DOU} = -D_{O_2}\frac{\mathrm{d}[O_2]}{\mathrm{d}z}, \quad (2)$$

where z is the depth and $[O_2]$ denotes O_2 concentration. The slope $\mathrm{d}[O_2]/\mathrm{d}z$ was determined from the gradient in the diffusive boundary layer (Glud, 2008), and while profiling, the overlying water was bubbled with air to ensure a water flow over the sediment surface. The molecular diffusion coefficient of O_2 in seawater (D_{O_2}) was calculated as a function of the bottom water salinity and temperature using the CRAN:marelac extension package in the R open-source programming language (Soetaert et al., 2010).

2.6 Statistical analyses

Results are reported as the mean ± 1 standard deviation (SD) of n replicate measurements. Nonparametric statistics were used in the interpretation of results, including the Mann–Whitney U test (p) for comparison of the mean of two independent groups of measurements. The Spearman rank correlation coefficient (ρ) was used as a measure of the statistical dependence between two variables X and Y. The more frequently used Pearson correlation provides a measure of the linear relationship between two continuous random variables, while Spearman's correlation allows nonlinear correlation. More precisely, a perfect Spearman correlation results when X and Y are related by any monotonic function, while for the Pearson correlation, a perfect correlation only results when X and Y are related by a linear function. As the environmental variables tested were nonlinearly related (see Fig. 8), we used the Spearman correlation. Statistical analyses were conducted in R using the CRAN:stats package.

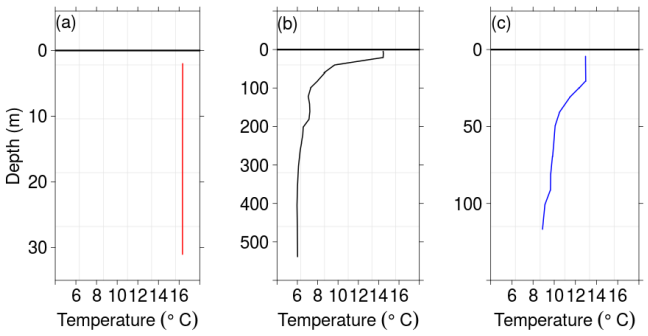

Figure 2. Temperature profiles as recorded by a CTD cast for **(a)** Station 11 (SNS), **(b)** Station 65 (SKNT), and **(c)** Station 80 (NNS).

3 Results

3.1 Bottom water characteristics

Bottom water salinity, temperature and oxygen concentration as obtained by CTD profiling are listed in Table 1, and characteristic temperature depth profiles are displayed in Fig. 2. Bottom water salinity and temperature of stations from the basin-wide North Sea cruise ranged from 35.12 PSU (NNS) to 33.01 PSU (SNS) and from 16.36 °C (SNS) to 6.13 °C (NNS). The bottom water in the NNS and SKNT was generally colder and more saline than bottom water in the SNS (Mann–Whitney; temperature: $p = 0.001$; salinity: $p < 0.001$). A thermocline was formed between 20 and 50 m water depth in all stations of the NNS and SKNT (Fig. 2 and Table 1). As noted above, the absence of stratification was used to classify stations within the SNS. The bottom water oxygen concentrations did not however exhibit significant differences between the SNS and other parts of the North Sea (Mann–Whitney; $p > 0.5$).

3.2 Sediment properties

The median grain size for all stations visited during the basin-wide North Sea campaign in 2011 ranged from 28 to 499 µm

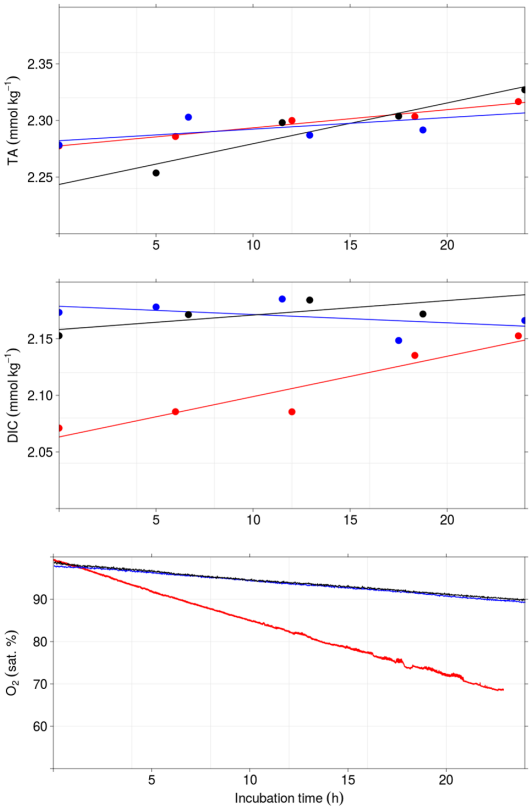

Figure 3. Representative concentrations of A_T, DIC and O_2 saturation over time for all three regions of the North Sea. Red: Station 11 (SNS); blue: Station 71 (NNS); black: Station 65 (SKNT).

(mean median grain size: 215 µm). In the SNS the median grain size ranged from 138 to 499 µm (mean median grain size: 263 µm), and according to the Wentworth scale, the SNS sediments can be classified as fine to medium sand (Table 1). Sediments in the NNS (median grain size range: 119–314 µm; mean: 225 µm) were not significantly different from the SNS (Mann–Whitney; $p = 0.8$), hence also being classified as fine to medium sand. In contrast, sediments from the Skagerrak and Norwegian Trench (SKNT) were considerably finer (Mann–Whitney; $p < 0.01$), with the median grain size ranging from 21 to 62 µm. Thus, sediments of SKNT are classified as fine to coarse silt on the Wentworth scale (Table 1).

Porosity for all stations in the North Sea basin varied from 0.32 to 0.74. Between sediments of the SNS (mean: 0.35) and NNS (mean: 0.35), no significant differences in porosity were found (Mann–Whitney; $p = 0.31$). However, sediments of the SKNT displayed a significantly higher porosity (mean: 0.68) than sediments from the SNS or NNS (Mann–Whitney; $p < 0.05$).

3.3 Benthic flux chamber incubations

The concentration changes over time of O_2, DIC, and A_T in the overlying water from flux chamber incubations are presented in Fig. 3 for representative stations from each of the three zones (SNS, NNS, SKNT). Stations were chosen to represent average benthic fluxes for the respective region of the North Sea, thus not considering stations that are likely to underestimate or overestimate benthic fluxes (e.g., Station 20). The oxygen data display a linear decrease, while the DIC and A_T data display a increasing trend, albeit with greater variability due to the limited number of subsamples (four or five). Fluxes were only included in further analysis if their calculation is based on a linear regression of at least four points combined with an r^2 value greater than 0.8. Furthermore, fluxes were set to zero in case the slope of the linear regression was not significantly different from zero.

During the basin-wide campaign in September 2011, TOU rates ranged from 3.1 to 28.7 mmol m^{-2} d^{-1} for the SNS, 0.7 to 6.2 mmol m^{-2} d^{-1} for the NNS, and 2.9 to 5.7 mmol m^{-2} d^{-1} for the SKNT. During the Dutch transect cruise in June 2012, TOU rates ranged from 6.5 to 25.1 mmol m^{-2} d^{-1} (Table 2). Thereby, the highest oxygen uptake rates were measured in the SNS, followed by the SKNT, while the lowest TOU rates were measured in the NNS (mean SNS values: 10.3 mmol m^{-2} d^{-1} in 2011 and 13.5 mmol m^{-2} d^{-1} in 2012; SKNT: 3.9 mmol m^{-2} d^{-1}; NNS: 3.2 mmol m^{-2} d^{-1}). In general, TOU rates in the SNS are significantly higher than TOU rates of the NNS and the SKNT (Mann–Whitney; NNS: $p < 10^{-5}$; SKNT: $p < 0.001$). Between TOU rates from the NNS and SKNT, no statistical difference could be identified (Mann–Whitney; $p = 0.6$). Furthermore, TOU rates measured in the SNS in June 2012 are not significantly different from TOU rates measured in September 2011 (Mann–Whitney; $p > 0.05$).

Within the permeable sediments of the SNS and NNS, flux chamber incubations were performed at two different stirring speeds (40 and 80 rpm). The TOU values at these two stirring speeds were linearly correlated (Fig. 4a). In general, the TOU rates were about 80 % higher at the higher stirring speed, indicating that the pore-water transport was dominated by physical advection, as expected in permeable sediments. On the other hand, a correlation between median grain size of the sediments and TOU rates could not be confirmed.

In general, A_T and DIC concentrations increased linearly with time in the overlying water of the flux incubations for most stations. A_T fluxes for both campaigns ranged from 0 to 21.4, 0 to 3.0 and 1.4 to 9.9 mmol m^{-2} d^{-1} for the SNS, NNS and SKNT, respectively. The highest A_T fluxes were observed in the SNS (mean: 6.6 mmol m^{-2} d^{-1} in 2011 and 5.7 mmol m^{-2} d^{-1} in 2012) and in the SKNT (4.3 mmol m^{-2} d^{-1}). The lowest mean A_T flux was calculated for the NNS (1.7 mmol m^{-2} d^{-1}). Only the A_T fluxes of the SNS are significantly higher than A_T fluxes of the NNS (Mann–Whitney; SNS: $p < 0.001$; SKNT: $p = 0.3$).

Table 2. Fluxes at the sediment–water interface for O_2 (TOU), A_T, and DIC. [a] Hydes et al. (1999); [b] Thomas et al. (2009). Units mmol C m^{-2} d^{-1} (DIC flux), mmol m^{-2} d^{-1} (A_T flux), and mmol O_2 m^{-2} d^{-1} (TOU rate).

		September 2011		June 2012		Literature	
		Mean	Range	Mean	Range	Mean	Range
TOU	SNS	10.3 ± 2.4	3.1–28.7	13.5 ± 4.5	6.5–25.1	14.9[a]	5.2–28.4[a]
	NNS	3.2 ± 0.4	0.7–6.2	–	–	–	–
	SKNT	3.9 ± 0.4	2.9–5.7	–	–	–	–
A_T	SNS	6.6 ± 5.2	0–21.4	5.7 ± 3.7	0.5–18.7	9.6[b]	–
flux	NNS	1.7 ± 2.4	0–3	–	–	–	–
	SKNT	4.3 ± 3.3	1.4–9.9	–	–	–	–
DIC	SNS	11.7 ± 5.5	1.5–29.1	12.3 ± 2.6		–	–
flux	NNS	0.8 ± 2.1	0–6.2	–	–	–	–
	SKNT	6.14 ± 2.6	4.2–7.4	–	–	–	–

A_T fluxes measured during the basin-wide cruise in 2011 are similar to those measured along the Dutch transect in 2012 (Mann–Whitney; $p = 0.3$).

DIC fluxes varied between 1.5 and 29.1, 0 and 6.2, and 4.2 and 7.2 mmol m^{-2} d^{-1} for the SNS, NNS, and SKNT, respectively. The trends in DIC flux were similar to those obtained for the TOU rates and A_T fluxes. The highest DIC fluxes were measured in the SNS, followed by the SKNT and the NNS (mean: SNS: 11.7 mmol m^{-2} d^{-1} in 2011 and 12.3 mmol m^{-2} d^{-1} in 2012; SKNT: 6.1 mmol m^{-2} d^{-1}; NNS: 0.8 mmol m^{-2} d^{-1}). DIC fluxes were significantly higher in the SNS than in the NNS, but showed no differences to the DIC fluxes measured in the SKNT (Mann–Whitney; NNS: $p < 0.01$; SKNT: $p = 0.3$), while no significant difference was found either between DIC fluxes of the SKNT and the NNS (Mann–Whitney; $p = 0.08$). As found for TOU rates and A_T fluxes, the DIC fluxes in the SNS were similar between both campaigns (Mann–Whitney; $p = 0.7$). This allows us to examine all solute fluxes recorded in the SNS as one single group in the discussion section.

3.4 O_2 and pH microprofiling

Representative examples of O_2 and pH depth profiles in stations from all three zones of the North Sea are presented in Fig. 5. In some stations pore-water profiles could not be measured due to the coarse grain size and the presence of carbonate shell fragments, which induce a high risk of damaging the microsensors. In general, pore-water O_2 declines as a result of O_2 consumption associated with organic matter degradation. From the O_2 depth profiles the DOU rates of the sediments were calculated as detailed in Sect. 2.5. In the SNS, DOU rates ranged from 0.20 to 6.95 mmol m^{-2} d^{-1}, while in the NNS and SKNT, ranges of 1.47 to 4.33 and 0.83 to 2.49 mmol m^{-2} d^{-1} were found (Table 3). The lowest mean DOU rate was measured in the SKNT, followed by the DOU rates of the NNS and SNS (SKNT: 1.77 mmol m^{-2} d^{-1}; NNS: 1.92 mmol m^{-2} d^{-1}; SNS: 3.08 mmol m^{-2} d^{-1}).

Table 3. Comparison between TOU rates as measured by FireSting optodes and diffusive oxygen uptake rates (DOU) obtained from O_2 microprofiles. Unit: mmol O_2 m^{-2} d^{-1}; oxygen penetration depth (OPD) for cores used for microprofiling in mm. NA indicates that oxygen does not deplete over the measured depth.

Station	TOU	DOU	OPD
11	10.02	0.20	NA
20	22.40	2.07	6.8
30	11.33	6.95	2.6
38	3.73	1.06	15.8
45	7.32	1.67	NA
52	5.49	0.83	19.0
56	3.76	1.47	NA
59	4.94	4.33	5.2
62	4.80	2.49	NA
65	3.01	1.88	16.4
71	3.67	1.76	7.4
80	4.62	1.25	10.8
88	2.25	1.87	18.8

The oxygen penetration depth (OPD) is defined as the thickness of the oxic zone in marine sediments (Cai and Sayles, 1996), and was operationally defined as the depth below which the O_2 concentration drops below 1 µmol kg^{-1}. In some permeable sediments, the oxygen did not fully deplete over the measured depth profiles (first 2 cm), and so the OPD could not be determined. In the remaining cores, the OPD was as shallow as 4.7 ± 2.8 mm for the SNS, 18.1 ± 1.4 mm for the SKNT, and 9.8 ± 3.9 mm for the NNS.

Table 3 compares the TOU with the corresponding DOU for the basin-wide campaign in September 2011. The TOU / DOU ratio ranged from 50.1 (SNS) to 1.1 (NNS), and DOU rates were significantly lower than TOU rates (Spearman; $p < 0.01$), indicating that physically or biologically driven advective transport strongly enhanced the sedimentary oxygen uptake.

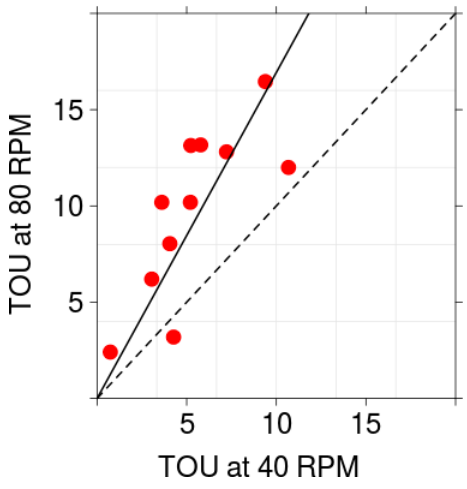

Figure 4. Total oxygen uptake rates measured in benthic incubation chambers at two different stirring rates (RPM: pounds per minute); dashed line: 1 : 1 line; solid line: linear regression; red symbols: SNS. All rates in mmol O_2 m^{-2} d^{-1}.

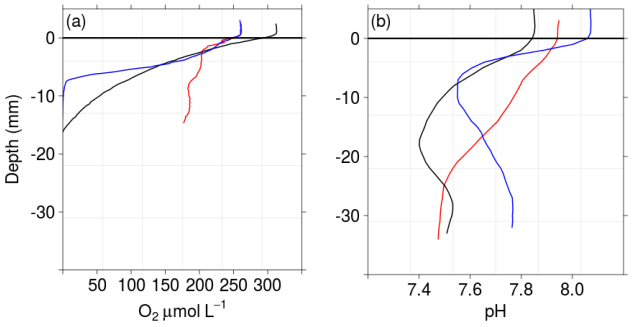

Figure 5. Examples of microsensor depth profiles from different regions of the North Sea. **(a)** O_2; **(b)** pH; red: Station 11 (SNS); blue: Station 65 (SKNT); black: Station 80 (NNS); solid line: sediment–water interface.

Depth pH profiles of representative cores are presented in Fig. 5. Depth profiles generally show a decline of pH in all profiled cores, which can be attributed to the release of CO_2 resulting from organic matter degradation. Furthermore, the cores from the NNS and SKNT were typically characterized by a sub-surface minimum in pH, while the depths of these pH minima matched the corresponding OPD. Hence, we interpret these sub-surface pH minima as resulting from the aerobic oxidation of reduced substances transported upwards from deeper sediment layers. Generally, the pH increased again at depth in the cores, most likely due to A_T generation associated with the anoxic degradation of organic matter (see discussion below).

4 Discussion

4.1 Benthic mineralization in the North Sea

Several studies have previously addressed benthic oxygen consumption in the North Sea, although most studies are restricted to the southern North Sea (Table 4). All TOU rates presented in the following section are not subdivided between both stirring speeds, but are discussed together. The TOU rates found in the present study for the North Sea (range 3.1–28.7 mmol O_2 m^{-2} d^{-1}) fall within the range of previously published TOU rates (range 0–57.1 mmol O_2 m^{-2} d^{-1}), which is however large. Due to temporal variability (seasonality), spatial variability (e.g., substrates ranging from cohesive mud to highly permeable sand), but also differences in methodology (see the discussion below on the impact of the stirring rate), it remains difficult to intercompare the oxygen consumption rates that have been obtained in different studies. So despite this growing database of TOU rates, a more accurate assessment of the spatial and temporal variation of the oxygen consumption in the North Sea remains an important challenge.

In our basin-wide campaign in 2011, we obtained the highest mean TOU rate in the SNS (10.3 mmol m^{-2} d^{-1}), followed by the SKNT (3.9 mmol m^{-2} d^{-1}), while the lowest TOU rates were measured in the NNS (3.2 mmol m^{-2} d^{-1}). One important environmental factor in controlling the TOU rates is the amount of primary production in these different regions. Part of this organic matter produced during photosynthesis is respired in the water column, while the remaining part sinks down to the sediments and undergoes respiration there. As oxygen serves as the ultimate electron acceptor for almost all respired organic carbon (Thamdrup and Canfield, 2000), high primary production rates tend to relate to high TOU rates in the sediments. Note that besides primary production rates, the water depth and thereby the amount of organic carbon that reaches the sediments are also of great importance. Because of the shallow water depth, the fraction of organic carbon that reaches the sediments in the southern North Sea is considerably higher than in the northern North Sea, hence further increasing the TOU rates in the SNS (Kühn et al., 2010). Based on measured surface chlorophyll concentration in the southern North Sea, Joint and Pomroy (1993) estimated primary production rates for a period from August 1988 to October 1989, and found clear regional differences in primary production in the SNS ranging from 18 mmol C m^{-2} d^{-1} along the British coast to 59 mmol m^{-2} d^{-1} in the German Bight. A model study by Moll (1998) covering the whole North Sea confirmed the large regional variation in depth-integrated annual primary production rates ranging from 21 mmol C m^{-2} d^{-1} in the NNS to 79 mmol C m^{-2} d^{-1} in the German Bight of the SNS. TOU rates observed are congruent with these previous observational and modeling studies, with high values in the south-

Table 4. TOU rates (mmol O_2 m^{-2} d^{-1}) measured in the North Sea and other coastal systems taken from the literature compared to this study. OG: Oyster Ground; FF: Frisian Front; DB: Dogger Bank; BF: Broad Fourteens; U1–U3: (near) English Channel; U4–U6: central North Sea; F115bis, F330, BM, BFS, BS: Belgian coast; Thms: Thames; USP: Outer Silver Pit; MS: Mediterranean Sea; FS: Faroe Shelf; WS: Washington Shelf; BC: northern Bering and Chukchi seas; SD: San Diego Trough; AC: Arctic continental slope; AS: Arabian Sea; MB: Monterey Bay; BS: Black Sea; AP: western Antarctic Peninsula; CS: Celtic Sea; SNS: southern North Sea; NNS: northern North Sea.

Literature North Sea	Location	Month and year	TOU
de Wilde et al. (1984)	OG	5, 8, 9 (1980, 1981)	3.6–14.4
Cramer (1990)	FF	5, 6 (1986), 8, 9 (1987)	23.3–51.8
Van Raaphorst et al. (1990)	DB	7, 8 (1988)	4–20
	BF	1, 4, 5, 8, 11 (1989)	2–22
Van Duyl et al. (1992)	FF	1, 4, 5, 8, 11 (1989)	15–40
Upton et al. (1993)	U1	9, 10 (1988), 2, 4, 6, 8, 9 (1989)	5–16
	FF	9, 10 (1988), 2, 4, 6, 8, 9 (1989)	5–28
	U3	9, 10 (1988), 2, 4, 6, 8, 9 (1989)	7–25
	U4	9, 10 (1988), 2, 4, 6, 8, 9 (1989)	10–11
	U5	9, 10 (1988), 2, 4, 6, 8, 9 (1989)	6–10
	U6	9, 10 (1988), 2, 4, 6, 8, 9 (1989)	7–18
Lohse et al. (1996)	OG	7 (1994)	5.6–6.1
Osinga et al. (1996)	BF	2 (1993), 7, 10 (1994)	< 24
	OG	2 (1993), 7, 10 (1994)	< 63
Boon et al. (1998)	BF	2, 3, 4, 6, 8, 11 (1993)	< 19.2
	FF	2, 3, 4, 6, 8, 11 (1993)	< 48
Trimmer et al. (2000)	Thms	7, 10 (1996), 4, 7 (1997)	11.4–5.8
Trimmer et al. (2005)	USP	10 (2001), 7 (2002)	16.1–57.1
	Thms	10 (2001), 7 (2002)	14–43.9
Weston et al. (2008)	OG	9 (2003)	12.6–30.6
Franco et al. (2010)	F115bis	2, 4, 10 (2003)	5.5–18.8
	F330	2, 4, 10 (2003)	1.2–8.7
Provoost et al. (2013)	F115	9, 10, 11, 12 (2002), 1, 2, 3, 4, 5, 7, 8, 9, 10 (2003)	4.5–32.9
Braeckman et al. (2014)	BM	2, 3, 4, 5, 6, 7, 8, 9 (2011)	0–41.92
	BFS	2, 3, 4, 5, 6, 7, 8, 9 (2011)	< 56.31
	BFS	10 (2011)	43.88
	BS	2, 3, 4, 5, 6, 7, 8, 9 (2011)	< 22.94
	BS	10 (2011)	6.63
Other coastal systems			
Lansard et al. (2008)	MS	06 (2001 and 2002)	3.9–25.6
Nordi et al. (2013)	FS	04 05 06 07 08 (2011) 02 06 07 (2012)	3.3–6.8
Archer et al. (1992)	WS	06 (1988)	1.0–18.3
Grebmeier and McRoy (1989)	BC	07 08 09 (1984–1986)	0.3–16.9
Smith Jr. (1974)	SD	10 (1973)	0.4–3.9
Boetius and Damm (1998)	AC	08 09 (1993)	0.2–2.3
Witte and Pfannkuche (2000)	AS	10 (1995)	0.9–6.3
Devol and Christensen (1993)	WS	06 07 (1988) 06 (1991)	2.9–18.5
Berelson et al. (2003)	MB	06 (1991)–10 (1995)	5.1–13.5
Friedl et al. (1998)	BS	Summer (1995)	0.0–33.0
Hartnett et al. (2008)	AP	03 06 10 (2000) 02 (2001)	1.5–2.1
Larsen et al. (2013)	CS	07 (2008	5.8–9.0
This study	SNS	9 (2011)	3.12–28.65
	SNS	6 (2012)	6.50–25.11
	NNS	9 (2011)	0.74–6.20

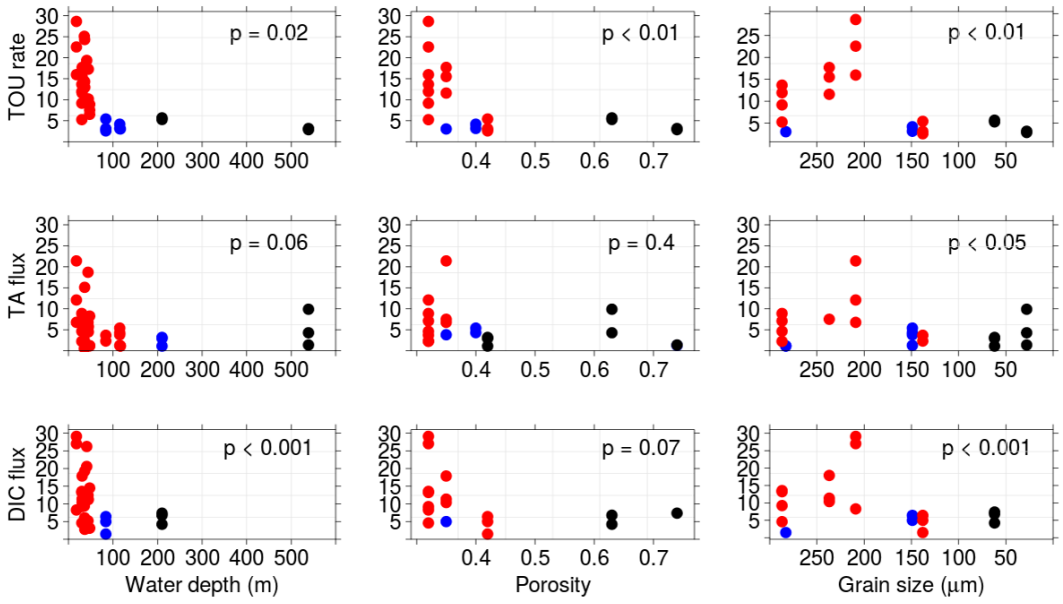

Figure 6. Correlation plots between DIC fluxes, A_T fluxes, TOU rates and water depth, porosity and grain size. Red: SNS; black: SKNT; blue: NNS. Spearman's p value given in each plot. Units mmol C m^{-2} d^{-1} (DIC), mmol m^{-2} d^{-1} (A_T), and mmol O_2 m^{-2} d^{-1} (TOU).

ern North Sea, and in particular in the German Bight, and lower values in the northern North Sea.

A second important environmental factor controlling the north–south gradient in TOU rates is the bottom temperature, which exhibits a similar gradient in summer, with higher temperatures in the south. In a recent seasonal flux study of shallow coastal sediments from the North Sea, a positive correlation was found between benthic solute fluxes and water temperature (Rao et al., 2014). These authors proposed that higher bottom water temperatures in summer are a main driver for higher benthic fluxes, as increased temperatures enhance the metabolic activity in the sediment. In September 2011, the thermocline was formed between 20 and 50 m (Fig. 2 and Sect. 3.1), and the whole NNS and SKNT were stratified, while in contrast, the SNS was fully mixed (which is the basis of our station classification). As a result, the bottom water in the NNS and SKNT was substantially cooler than bottom water in the SNS ($\approx 11\,^{\circ}$C difference between SNS and NNS/SKNT – Table 1). Adopting a temperature Q_{10} coefficient of ≈ 2 for benthic respiration (Denman and Pena, 2002; Schrum et al., 2006), one would expect a nearly doubling of the TOU between the NNS and SNS due to bottom water temperature, all other environmental factors being the same. Accordingly, lower bottom water temperatures in the NNS and SKNT could indeed partially explain the lower TOU values recorded compared to the SNS (Table 3).

To further identify the drivers of the observed spatial variability across the North Sea, we examined the correlation of TOU rates with water depth, porosity and grain size (Fig. 6). We found significant correlations between TOU values and water depth (Spearman; $p < 0.01$), suggesting that increased water depth reduced the benthic pelagic coupling in the NNS and SKNT. As more organic matter is remineralized upon the longer transit through the water column, less detritus reaches the seafloor, and this hence decreases the contribution of benthic mineralization in the overall respiration. Finally, we also found both a negative correlation between TOU and porosity (Spearman; $p < 0.02$) and a significant negative correlation between TOU and median grain size (Spearman; $p < 0.01$). This contradicts the classical picture of sedimentary diagenesis, where high oxygen consumption rates and intense biogeochemical cycling are typically linked to fine-grained organic-rich sediments. Instead, we found the highest TOU values in the permeable sediments of mostly the SNS (low porosity, high median grain size), which supports the more recent ideas of permeable sediments as active bio-catalytic filters (Huettel and Rusch, 2000), which actively trap suspended detritus by means of advective currents through the upper sediment layers and rapidly mineralize this trapped organic matter. As a result, these permeable sediments display low standing stocks of organic matter but high TOU values.

The importance of wind- and tidal-induced advective transport for the benthic oxygen dynamics is emphasized by the deep oxygenation of the surface sediment at permeable sites (Fig. 5a), the strong impact of benthic chamber stirring speed on the TOU (Fig. 4), and by the difference between TOU values as measured by benthic incubations and the corresponding DOU values as obtained by microprofiling (Table 3). We found that DOU values were always smaller than TOU values for all stations throughout the North Sea. In general, the total oxygen uptake can be decomposed as TOU = DOU + BMU + AMU (Glud, 2008), where BMU

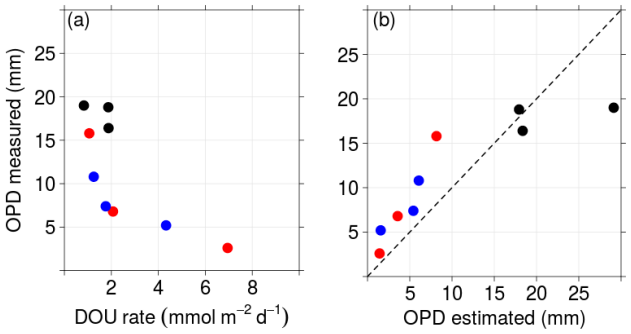

Figure 7. (a) Oxygen penetration depth (OPD) plotted versus diffusive oxygen uptake (DOU) rate. **(b)** Correlation between measured OPD and theoretical OPD. Dashed line: 1 : 1 line; red symbols: SNS; blue symbols: NNS; black: SKNT. For calculation and details, see the text.

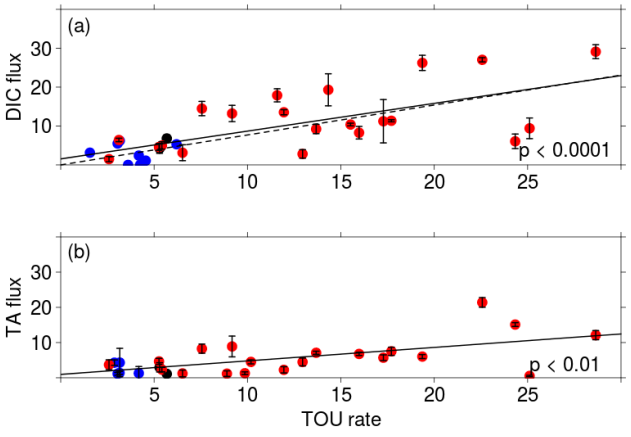

Figure 8. (a) Correlation between DIC fluxes and TOU rates. **(b)** Correlation between A_T fluxes and TOU rates. Solid line: linear regression; Spearman's p value given in each plot. TA and DIC fluxes in mmol C m^{-2} d^{-1}. TOU rates in mmol O_2 m^{-2} d^{-1}.

represents benthos mediated O_2 uptake resulting from burrow irrigation and the respiration of infauna, and AMU represents the advection mediated O_2 uptake by purely physical transport processes, such as pore-water advection induced by currents over bottom topography (Huettel and Rusch, 2000; Meysman et al., 2007) and oscillatory pore-water mixing induced by waves (Shum, 1992).

A second signature of physical and or biological pore-water irrigation is the deep oxygenation of the surface sediment. As already noted above, in some highly permeable sites, the surface sediment remained completely oxygenated over the whole surface layer that was examined by O_2 microsensor profiling (first 20 mm), and so no oxygen penetration depth (OPD) could be determined. For those stations that did allow one to determine the OPD (i.e., the pore-water O_2 signal decreased to zero), we employed the analytical model of Cai and Sayles (1996), which provides an inverse relation

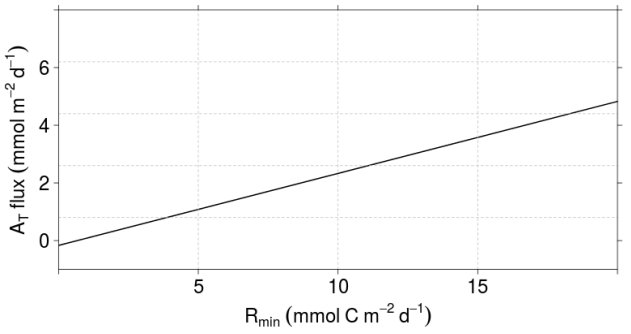

Figure 9. Sensitivity of the benthic A_T flux (dashed line) and the net A_T generation (solid line) towards a range of mineralization rates in the SNS.

between OPD and DOU (Fig. 7a) (Eq. 3).

$$L = 2\phi D_s \frac{[O_2]_{bw}}{F^0_{O_2}} \quad (3)$$

In this expression, L is the theoretical OPD of the sediment, ϕ is the porosity, and D_s is the effective diffusivity of O_2 in the pore water (i.e., corrected for tortuosity); $[O_2]_{bw}$ is the bottom water concentration of O_2 and $F^0_{O_2}$ is the benthic oxygen flux (i.e., the DOU). This relationship is based on the balance between diffusive oxygen fluxes and oxygen consumption rates under steady-state conditions and negligible advection. The above relation was used to estimate the theoretical OPD from the measured DOU as shown in Fig. 7b. The actually measured OPD is systematically larger than the predicted OPD for all stations (with SKNT stations 52 and 65 being the exception to this rule). As Eq. (3) holds for sediments that only experience diffusive transport, the discrepancy suggests that non-diffusive transport (i.e., bio-irrigation or physical advection) increases the oxygen availability and penetration in the sediment (Archer and Devol, 1992).

4.2 Benthic DIC release in the North Sea

The benthic DIC release in the North Sea follows the same spatial pattern as the benthic oxygen uptake: the highest DIC effluxes were recorded in the SNS (mean: 11.7 mmol m^{-2} d^{-1} in 2011 and 12.3 mmol m^{-2} d^{-1} in 2012), followed by the SKNT (mean: 6.1 mmol m^{-2} d^{-1}) and the NNS (mean: 0.8 mmol m^{-2} d^{-1}; Table 2). However, while TOU values were comparable in the NNS and SKNT, the DIC flux in the SKNT was significantly higher than in the NNS. As for the TOU, we found a significant positive correlation between the DIC efflux and water depth (Spearman; $p = 0.02$), and a weak negative correlation between the DIC efflux and the porosity (Spearman; $p = 0.07$) and a significant negative correlation between the DIC efflux and median grain size (Spearman; $p < 0.01$; Fig. 6). Overall, this suggests that the same environmental factors (pelagic primary production, temperature, water depth, sediment permeabil-

ity) that are driving the TOU are also controlling the spatial pattern of the sedimentary DIC release in the North Sea.

Overall, we found DIC fluxes to be positively correlated with TOU rates (Fig. 8a; Spearman; $p < 0.0001$). The ratio between the DIC efflux and the TOU at a given site represents the respiratory quotient (RQ), and we found that the mean RQ value for the SNS (0.95), NNS (0.94), and SKNT (1.00) to be all similar. No significant differences were detected between the three zones (Mann–Whitney; $p > 0.05$). In general, the RQ can be used as an indicator of the degree of reoxidation of reduced compounds associated with anaerobic remineralization (Therkildsen and Lomstein, 1993). Assuming that (1) no carbonate dissolution occurs in the sediment, (2) that the stoichiometry of organic matter follows the Redfield ratio ($C:N:P = 106:16:1$; Redfield, 1958), and (3) that organic matter is oxidized using oxygen as the sole electron acceptor, one would obtain a RQ of 0.77 (solid line in Fig. 8a; Paulmier et al., 2009). Note that a RQ close to the Redfield ratio serves as a baseline for comparison rather than an expected result in this study, due to the anticipated impact of anoxic respiration and carbonate dissolution. In principle, the RQ value is expected to increase with increasing importance of suboxic and anoxic respiration pathways, and subsequent accumulation of reduced compounds such as pyrite, as respiration along these pathways is releasing DIC without consuming oxygen. Alternatively, dissolution of carbonates may also lead to an increased RQ due to the release of 1 mole DIC per 1 mole $CaCO_3$ dissolved. Equally, the RQ value is expected to decrease when a stock of reduced compounds is being re-oxidized, i.e., the annihilation of a previously accumulated oxygen debt.

4.3 Benthic alkalinity release in the North Sea

Our results show that North Sea sediments can be a substantial source of A_T, with sediment effluxes ranging from 0 to 28.7 mmol m^{-2} d^{-1} (Fig. 8b). The A_T fluxes reported here were obtained by monitoring the temporal evolution of A_T in the overlying water of enclosed sediment incubations. In the same sediment incubations, Burt et al. (2014) measured the efflux of the short-lived radium isotopes (^{224}Ra and ^{223}Ra) and subsequently estimated A_T fluxes. To this end, these authors used the Ra-isotope data to estimate the overall water exchange rate between the pore water and the overlying water column. This water exchange rate was then multiplied by the excess concentration of A_T in pore water, which was estimated from pore-water analysis. This indirect estimate procedure resulted in benthic A_T fluxes between 4.7 and 22.1 mmol m^{-2} d^{-1}, and is in good agreement with the A_T flux values obtained here (Fig. 10). The disagreement (e.g., at Station 38) between observed and calculated A_T flux may result from applying the same A_T pore-water concentration for all stations in calculating the A_T fluxes based on Ra-isotope data. This assumption might be wrong and could lead to an overestimation of the A_T flux at Station 38. For a more detailed discussion on the correlation between both methods, see Burt et al. (2014).

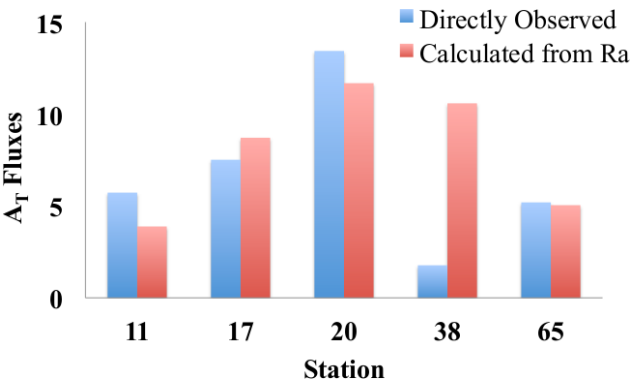

Figure 10. Directly measured A_T fluxes for the SNS compared to A_T flux estimations based on Ra measurements. Figure taken from Burt et al. (2014). Fluxes in mmol C m^{-2} d^{-1}.

The benthic A_T release in the North Sea follows the same spatial pattern as the benthic oxygen uptake and the DIC efflux, suggesting that organic matter mineralization is the primary driver for the A_T release from sediments. We observed the highest A_T release in the SNS (mean: 6.6 mmol m^{-2} d^{-1} in 2011 and 5.7 mmol m^{-2} d^{-1} in 2012), closely followed by the SKNT (mean: 4.3 mmol m^{-2} d^{-1}). The lowest A_T fluxes were obtained in the NNS (mean: 1.7 mmol m^{-2} d^{-1}). As for the TOU and DIC efflux, we found a weak positive correlation between A_T efflux and water depth (Spearman; $p = 0.06$), though no significant correlation between A_T efflux and porosity (Spearman; $p = 0.4$) and a significant negative correlation between the A_T efflux and median grain size (Spearman; $p < 0.01$) Fig. 6. The lack of negative correlation with porosity is mainly due to SKNT stations, which showed a high A_T efflux at high porosity. Furthermore, the increase in A_T fluxes with increasing TOU rates (Fig. 8) is an indication of metabolically driven dissolution of $CaCO_3$, as carbonate dissolution is fueled by CO_2 released during organic matter mineralization, or alternatively, of the increase in the relative importance of anoxic respiration pathways at high TOU. Metabolic dissolution would induce a A_T / DIC flux ratio of 1, which is indeed confirmed in some stations, though not for all (Fig. 11). A positive correlation is obtained between A_T and DIC fluxes (Spearman; $p = 0.02$), but there are marked differences in the A_T / DIC flux ratio between different stations, which suggests that a different type of biogeochemistry is acting at different locations. Below we will discuss in more detail how different biogeochemical processes in the sediment are releasing A_T and DIC in distinct ratios.

To our knowledge, the A_T fluxes presented here are the first field observations of such fluxes in the North Sea area. Thomas et al. (2009) estimated sedimentary A_T fluxes in the southeastern bight of the North Sea and the Wadden Sea during summer and autumn based exclusively on water column

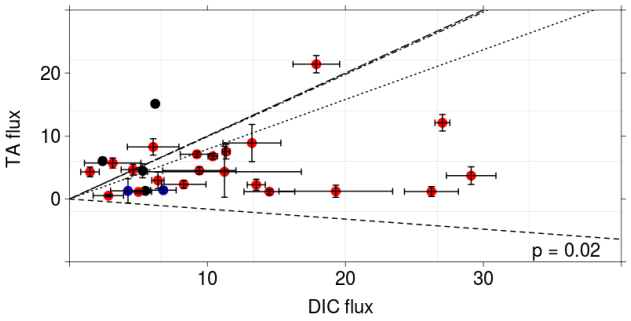

Figure 11. Correlation between A_T and DIC fluxes for sites of the SNS from both campaigns. Different lines represent different reaction stoichiometry. For more explanation and reaction equations, see the text. Short dashed line: aerobic respiration; dotted line: denitrification; dotted–dashed line: sulfate reduction coupled to pyrite formation and burial; long dashed line: carbonate dissolution. Note that the latter two lines are plotted along similar points and are thus hard to distinguish. p: Spearman's rank correlation coefficient for the correlation of all points displayed in this scatter plot. All fluxes in mmol C m^{-2} d^{-1}.

data. In this approach, the sedimentary A_T release appeared as the unknown closure term in an A_T budget based on water column data, which provided A_T flux estimates of about 8.0 mmol m^{-2} d^{-1}. These values are similar to the benthic A_T fluxes reported here for the SNS.

A_T release from sediments has also been the subject of a number of studies on coastal systems other than the North Sea. Based on basin-wide budget calculations, Gustafsson et al. (2014) estimated that sediments of the Baltic Sea generate A_T with a mean rate of 2.4 mmol m^{-2} d^{-1}, which is on the same order as the A_T input by rivers in that basin. As main sources of A_T, these authors propose denitrification together with sulfate reduction and/or silicate weathering. Chen and Wang (1999) estimated that sediments in the East China Sea generate between 2.9 and 4.9 mmol m^{-2} d^{-1} A_T. Over 80 % of this A_T flux was thereby attributed to iron and sulfate reduction, with no contribution from carbonate dissolution.

Krumins et al. (2013) used a one-dimensional reactive transport model to estimate A_T fluxes from coastal sediments. For that study, the authors divided the global shelf into four different environments, each with distinctive particular organic and inorganic carbon fluxes. Ultimately, they identified non-carbonate shelves (e.g., the North Sea) as an A_T source of 2.7 mmol m^{-2} d^{-1}.

On a global scale, Krumins et al. (2013) estimated an A_T flux for the coastal ocean of 29 Tmol yr^{-1}. Whereas this estimate agrees well with an independent estimation by Chen (2002) (16–31 Tmol yr^{-1}), Hu and Cai (2011a) obtained a much smaller flux of 4–6 Tmol yr^{-1}. Note that all these three studies are based on different assumptions about the underlying processes that are generating A_T. Whereas the A_T flux estimated by Chen (2002) is mainly generated by sulfate reduction with zero contribution of carbonate dissolution, Krumins et al. (2013) acknowledged carbonate dissolution as a benthic A_T source. The estimate of Hu and Cai (2011a) is based on anaerobic A_T generation alone; hence, possible contributions by carbonate dissolution are not taken into account. Furthermore, these latter authors treat the coastal sediment–water column system as a single system, while the other two papers only consider the sediment.

To put these different assumptions into perspective, and to verify their consequences, we now develop an alkalinity budget for the SNS in which we first provide a sediment budget, and subsequently we extend this argument to arrive at a combined sediment and water column alkalinity budget. We restrict this discussion to the SNS, as we have shown in Sect. 3.3 that A_T fluxes in the SNS significantly exceed those of the other two zones. High primary production, riverine input of terrestrial organic matter, and the shallow water depth favor a high benthic respiration rate in the SNS. Furthermore, in the context of atmospheric CO_2 uptake, a direct link between alkalinity release from the sediments and the atmosphere is needed, which requires a non-stratified water column as encountered in most parts of the SNS.

4.4 Sources of alkalinity in sediments of the SNS

The high benthic A_T effluxes observed in the SNS invoke the question of which processes generate A_T in the sediment. In the following we will discuss how different biogeochemical pathways contribute to the overall A_T release from sediments, and in this way, we will try to assemble a closed A_T budget for the SNS seafloor. To this end, we developed a simplified biogeochemical model of the SNS sediment, which accounts for carbonate dissolution (CD), aerobic respiration (AR), nitrification (NI), denitrification (DNF), iron reduction (IR), sulfate reduction (SR), free sulfide oxidation (SO), and pyrite formation (PF) as biogeochemical pathways. The input parameters, diagenetic relations, and output variables are summarized in Table 5. The A_T / DIC flux ratio for each of these reactions is indicated as a straight line in Fig. 11. In the next paragraphs, we discuss how the rates of the individual reactions can be constrained based on our flux measurements and literature data.

In theory, the dissolution of 1 mole of $CaCO_3$ releases 2 mole of A_T, assuming no other processes are acting.

$$CaCO_3 \rightarrow {CO_3}^{2-} + {Ca}^{2+} \quad (4)$$

The undersaturation of the pore water with respect to the phases of calcium carbonate present (e.g., high Mg calcite, aragonite or calcite) determines the rate at which carbonate will dissolve. In general the undersaturation of the pore water can have two causes (Boudreau et al., 2010): (1) undersaturation of the overlying water and (2) additional undersaturation of the pore water due to metabolic respiration. In the North Sea, the overlying water is always oversaturated with respect to all common carbonate phases (Frankignoulle et al.,

Table 5. Input parameters and rate expressions for all diagentic and pelagic processes included in our model. Additionally, the impacts of the different elemental cycles are expressed in percentages. For details on single reaction rates, see Sect. 4.4.

Input parameter	Expression	Value	Units	A_T release
Mineralization rate	R_{min}	10.3	mmol C m^{-2} d^{-1}	–
Aerobic respiration fraction	a	0.15	–	–
Fraction of DNF supported by NI	b	0.8	–	–
Pyrite formation fraction	p	0.1	–	–
Benthic fluxes				
–	$J_{NO_3} = (1-b) \times 0.8 \times DNF$	–	–	–
–	$J_{NH_4} = 0$	–	–	–
–	$J_{Fe^{2+}} = 0$	–	–	–
–	$J_{H_2S} = 0$	–	–	–
Balance statements				
–	$\delta[CO_2]/\delta t = +R_{min}$	–	–	–
–	$\delta[O_2]/\delta t = -AR - R_{SO} - R_{NIT}$	–	–	–
–	$\delta[NO_3]/\delta t = NIT - 0.8 \times DNF + J_{NO_3}$	–	–	–
–	$\delta[NH_4^+]/\delta t = a \times R_{min} - R_{NIT} + AM + J_{NH_4}$	–	–	–
–	$\delta[Fe^{2+}]/\delta t = 4 \times IR - \frac{1}{2} \times PF + J_{Fe^{2+}}$	–	–	–
–	$\delta[H_2S]/\delta t = 0.5 \times SR - PF - SO + J_{H_2S}$	–	–	–
Pelagic processes				
Primary production	PP	45.36	mmol C m^{-2} d^{-1}	+7.28
Aerobic respiration	WAR	36.11	mmol C m^{-2} d^{-1}	−5.79
Carbonate formation	CF	2.70	mmol C m^{-2} d^{-1}	−5.40
Nitrogen fixation	NF	0	mmol C m^{-2} d^{-1}	0
Alkalinity generation	See text	–	mmol m^{-2} d^{-1}	−3.92
Diagenetic processes				
Carbonate dissolution	CD = CF	2.70	mmol C m^{-2} d^{-1}	+5.40
Aerobic respiration	$AR = a \times R_{min}$	1.55	mmol C m^{-2} d^{-1}	+0.22
Ammonification	$AM = \frac{16}{106} \times R_{min}$	1.55	mmol N m^{-2} d^{-1}	–
Nitrification	NIT = AM	1.55	mmol N m^{-2} d^{-1}	−3.10
Denitrification	$DNF = \frac{1}{b} \times NIT \times \frac{106}{84.8}$	2.43	mmol C m^{-2} d^{-1}	+2.29
Sulfate reduction	$SR = (R_{min} - AR - DNF)/(\frac{1}{16} \times p + 1)$	6.29	mmol C m^{-2} d^{-1}	+7.18
Pyrite formation	$PF = 8 \times IR$	0.31	mmol C m^{-2} d^{-1}	−0.29
	$PF = 0.5 \times p \times SR$	0.31	mmol C m^{-2} d^{-1}	−0.29
Sulfide oxidation	$SO = 0.5(1-p) \times SR$	2.83	mmol C m^{-2} d^{-1}	−5.66
Iron reduction	$IR = \frac{1}{16} \times p \times SR$	0.04	mmol C m^{-2} d^{-1}	+0.32
Alkalinity generation	See text		mmol m^{-2} d^{-1}	+6.32
Total oxygen uptake	$TOU = AR + 2 \times NIT + 2 \times SO + 0.25 \times PF$	10.1	mmol O_2 m^{-2} d^{-1}	
Respiratory quotient	$RQ = \frac{R_{min}+CD}{TOU}$	1.25	–	–
A_T turnover linked to				
Carbon cycle	$2 \times CD - 2 \times CF$	0	%	–
Nitrogen cycle	$84.8/106 \times DNF + 16/106 \times (AR + DNF + IR + SR) - 2 \times NIT + (16/106) \times (PP - WAR)$	74	%	–
Sulfur and iron cycle	$8 \times IR + SR - 2 \times SO - PF$	26	%	–
Phosphor cycle	$-1/106 \times (AR+DNF+IR+SR) + (1/106) \times (PP - WAR)$	0	%	–

1998; Kühn et al., 2010), and so, dissolution of $CaCO_3$ in the sediment must be exclusively metabolically driven. Both the CO_2 production during organic matter mineralization as well as the oxidation of reduced compounds produced during anaerobic respiration processes can make the pore water undersaturated with respect to carbonates and, therefore, fuel metabolic driven dissolution (Jahnke et al., 1994). The increase in the A_T fluxes with increasing TOU rates (Fig. 8b) indeed forms an indication of metabolic driven dissolution of $CaCO_3$ (Jahnke and Jahnke, 2004).

From the flux data set available here, it is not possible to constrain the actual $CaCO_3$ dissolution rate in each station. However, it is still possible to provide an upper limit for the $CaCO_3$ dissolution rate on a larger geographic scale. Gazeau et al. (personal communication, 2014) recently estimated carbonate production in the southern North Sea to be $2.7\,\mathrm{mmol\,C\,m^{-2}\,d^{-1}}$. Net carbon burial does not occur in the North Sea, except for small amounts in the Skagerrak and the Norwegian Channel (de Haas et al., 2002; Thomas et al., 2005; Bozec et al., 2006). Therefore, we consider carbonate production (in both water column and sediment) and dissolution (in the sediment) to be in balance with each other. Accordingly, carbonate dissolution in sediments can release up to $5.4\,\mathrm{mmol\,m^{-2}\,d^{-1}}$ of A_T.

In addition to carbonate dissolution, A_T generation can be linked to various organic matter degradation pathways and secondary re-oxidation reactions. In the presence of oxygen, aerobic respiration is used to break down organic matter:

$$\mathrm{OM} + 15\mathrm{H^+} + 106\mathrm{O_2} \rightarrow 106\mathrm{CO_2} + 16\mathrm{NH_4^+} + \mathrm{H_2PO_4^-} + 148.4\mathrm{H_2O}, \quad (5)$$

where we assume organic matter (OM) to be of Redfield elemental composition and follow the classical expression for the composition of organic matter $(CH_2O)_{106}$ $(NH_3)_{16}$ (H_3PO_4) after Richards (1965) and Paulmier et al. (2009) (Redfield, 1958). This reaction essentially generates A_T by the consumption of protons linked to ammonium release, and to a lesser extent, it consumes A_T by the release of phosphate. Thamdrup and Canfield (2000) have estimated that aerobic respiration accounts for between 5 and 25 % of the total benthic mineralization in shelf and coastal sediments. If we adopt a value of the benthic mineralization rate $R_{\mathrm{min}} = 10.3\,\mathrm{mmol\,C\,m^{-2}\,d^{-1}}$, which is the mean TOU value recorded for the SNS in September 2011 (Table 2; see also the discussion below), we can estimate the aerobic respiration rate to range between 0.52 and $2.58\,\mathrm{mmol\,C\,m^{-2}\,d^{-1}}$ for the SNS (mean: $1.55\,\mathrm{mmol\,C\,m^{-2}\,d^{-1}}$). Accounting for stoichiometry (A_T/O_2 ratio $= 15/106$), the corresponding A_T release ranges from 0.09 to $0.37\,\mathrm{mmol\,m^{-2}\,d^{-1}}$, with a mean of $0.22\,\mathrm{mmol\,m^{-2}\,d^{-1}}$. A theoretical doubling of R_{min} would lead to a ≈ 7 % increase in the benthic A_T flux, and to a ≈ 115 % net A_T increase in the water column (Fig. 9), that is, if R_{min} is the only parameter changed and thus the relative importance between different diagenetic processes remains the same.

Nitrification of ammonium released during mineralization consumes A_T and can be represented by the reaction equation

$$\mathrm{NH_4^+} + 2\mathrm{O_2} \rightarrow \mathrm{NO_3^-} + \mathrm{H_2O} + 2\mathrm{H^+}. \quad (6)$$

Per mole of ammonium that is released during mineralization, exactly 2 mole of A_T are consumed. If we use the TOU as a proxy for R_{min} ($10.3\,\mathrm{mmol\,C\,m^{-2}\,d^{-1}}$), the rate of ammonification (i.e., $16/106\,R_{\mathrm{min}}$) becomes $1.55\,\mathrm{mmol\,N\,m^{-2}\,d^{-1}}$ for the SNS. If all the ammonium is re-oxidized, and hence no ammonium escapes the sediment, the nitrification rate should match the ammonification rate, and so the associated A_T consumption becomes $3.10\,\mathrm{mmol\,m^{-2}\,d^{-1}}$. Also note that complete aerobic respiration, i.e., the combination of aerobic respiration Eq. (5) with nitrification Eq. (6), consumes 17 mole A_T per 106 mole of DIC released.

Denitrification is a second mineralization pathway via which organic matter degradation proceeds in the sediment, and can be represented as

$$\mathrm{OM} + 84.8\mathrm{NO_3^-} + 99.8\mathrm{H^+} \rightarrow 106\mathrm{CO_2} + 42.4\mathrm{N_2} + 16\mathrm{NH_4^+} + \mathrm{H_2PO_4^-} + 106\mathrm{H_2O}. \quad (7)$$

Per mole C in POC (particulate organic carbon) denitrified, the A_T increases by $0.94 = 99.8/106$ mole. To discuss the impact of denitrification on sedimentary A_T release, we need to consider the origin of the nitrate that is used for denitrification. A portion of the nitrate is internally generated in the sediment through coupled nitrification–denitrification, while another part of the nitrate is derived externally (i.e., from the overlying water column). It has been estimated that these coupled nitrification–denitrification reactions account for 80 % of the total denitrification rates in coastal environments (Middelburg et al., 1996; Seitzinger et al., 2006), which thus implies that the total denitrification rate should scale as $1/0.8$ times the nitrification rate ($1.55\,\mathrm{mmol\,N\,m^{-2}\,d^{-1}}$). This way, we obtain a denitrification rate of $1.94\,\mathrm{mmol\,N\,m^{-2}\,d^{-1}}$ or $2.43\,\mathrm{mmol\,C\,m^{-2}\,d^{-1}}$, with an associated A_T release of $2.29\,\mathrm{mmol\,m^{-2}\,d^{-1}}$. In the North Sea, a tight coupling of nitrification and denitrification has indeed been reported by Lohse et al. (1993) and Pätsch and Kühn (2008), and observed benthic denitrification rates in the SNS range from 1.6 to $4.6\,\mathrm{mmol\,C\,m^{-2}\,d^{-1}}$ (Lohse et al., 1996; Hydes et al., 1999), a range that centrally embraces our estimate here. Note that the coupling of ammonification, nitrification and subsequently denitrification does not lead to net production of A_T. Only if nitrate is derived from the overlying water column does one obtain a net production of A_T in the pore water (Hu and Cai, 2011a).

Once nitrate and oxygen are fully consumed, dissimilatory iron reduction and sulfate reduction are the prevailing respiration pathways (in the SNS we assume manganese oxides to be a minor electron acceptor, and so we ignore this pathway).

$$\mathrm{OM} + 53\mathrm{SO_4}^{2-} + 121\mathrm{H}^+ \rightarrow 53\mathrm{H_2S} + 106\mathrm{CO_2} + 16\mathrm{NH_4}^+ + \mathrm{H_2PO_4}^- + 106\mathrm{H_2O} \quad (8)$$

$$\mathrm{OM} + 424\mathrm{FeOOH} + 863\mathrm{H}^+ \rightarrow 424\mathrm{Fe}^{2+} + 106\mathrm{CO_2} + 16\mathrm{NH_4}^+ + \mathrm{H_2PO_4}^- + 742\mathrm{H_2O} \quad (9)$$

Both reactions consume protons, and hence produce A_T. Per mole C in POC oxidized, sulfate and iron reduction release 1.14 and 8.14 mole of A_T, respectively. However, to assess the net A_T generation in the sediment, we need to take the fate of the reduced species into account. The free sulfide that is generated by sulfate reduction can follow two major pathways. Some of the free sulfide (fraction p) will react with the reduced iron liberated by iron reduction to form pyrite. Due to its thermodynamic stability, pyrite is considered to be the primary sink for both iron and sulfur on the timescales of early diagenesis (Hu and Cai, 2011a). Dissolved iron fluxes between the sediment and the overlying water column are considered to be low throughout the southern North Sea and are thus ignored for the following discussion (Slomp et al., 1997). The overall process of pyrite formation can be represented by the reaction equation

$$\frac{1}{2}\mathrm{Fe}^{2+} + \frac{1}{4}\mathrm{O_2} + \mathrm{H_2S} \rightarrow \frac{1}{2}\mathrm{FeS_2} + \mathrm{H}^+ + \frac{1}{2}\mathrm{H_2O}. \quad (10)$$

First, reduced iron reacts with HS^- to form FeS, and in a second step the produced FeS reacts with $\mathrm{H_2S}$ to form pyrite ($\mathrm{FeS_2}$) Hu and Cai (2011b). The remaining part of the free sulfide generated by sulfate reduction (fraction $1-p$) is transported upwards towards the oxic zone and re-oxidized with oxygen:

$$\mathrm{H_2S} + 2\mathrm{O_2} \rightarrow \mathrm{SO_4}^{2-} + 2\mathrm{H}^+. \quad (11)$$

Both pyrite formation and free sulfide reoxidation consume alkalinity. However, when combined with the alkalinity impact of sulfate reduction, pyrite formation results in a net generation of alkalinity, while the alkalinity consumed in free sulfide reoxidation exactly compensates for the alkalinity generated during sulfate reduction. Thamdrup et al. (1994) calculated for sediments of Aarhus Bay that the burial of reduced sulfur accounts for only 20 % of the total sulfate reduction rate, and similar values are reported in other studies (Jørgensen, 1977; Berner and Westrich, 1985; Jørgensen et al., 1990). The sediments of SNS are generally coarser and more permeable than those of Aarhus Bay, which leads to more advection and reoxygenation, which favors sulfide reoxidation as opposed to pyrite formation. Therefore, here we adopt a reduced degree of pyrite formation (10 %; Table 5).

Adopting steady state, our simplified diagenetic model provides a set of linear relations (Table 5), which generate a particular division of the total organic matter mineralization into aerobic respiration (15 %), denitrification (24 %), iron reduction (0.4 %), and sulfate reduction (61 %). These estimates are comparable to the model analysis of Krumins et al. (2013), who estimated that sulfate reduction is the main respiratory pathway on continental shelves, accounting for 77–85 % of the organic matter mineralization, followed by aerobic respiration (16 %), denitrification (2–4 %) and iron reduction (0.3–0.7 %). Similarly, Nedwell et al. (1993) estimated that sulfate reduction accounted for 10–53 % of the total organic matter mineralization in the SNS, while a coupled benthic–pelagic model for the North Sea suggests that up to 30 % of the organic matter is mineralized using sulfate as the electron acceptor (Luff and Moll, 2004). The TOU rate predicted by the model (10.4 mmol $\mathrm{O_2\,m^{-2}\,d^{-1}}$) agrees well with the mean TOU observed in the SNS in September 2011 (10.3 mmol $\mathrm{O_2\,m^{-2}\,d^{-1}}$), but the predicted respiratory coefficient (RQ = 1.25) is higher than the observed one (RQ = 0.95). This higher simulated RQ could be due to an overestimate of carbonate dissolution rate. However, such a reduction of the carbonate dissolution rate would at the same time lead to a substantial underprediction of the sedimentary alkalinity release, and so we stick to the carbonate dissolution rate CD = 2.7 mmol $\mathrm{C\,m^{-2}\,d^{-1}}$.

Accounting for the contributions of all biogeochemical reactions as discussed in this section above, the total alkalinity generation in the sediment R_sed becomes (Fig. 12)

$$R_\mathrm{sed} = 2r_\mathrm{CD} + \frac{16-1}{106}r_\mathrm{AR} + \frac{84.8+16-1}{106}r_\mathrm{DNF} + \frac{848+16-1}{106}r_\mathrm{IR} + \frac{106+16-1}{106}r_\mathrm{SR} - 2r_\mathrm{NIT} - 2r_\mathrm{SO} - r_\mathrm{PF}. \quad (12)$$

Note that all the calculations are based on measurements carried out in June and September, and thus care should be taken when transferring these rates to an annual scale. As we assume no alkalinity flux to deeper sediment layers, the total alkalinity generation in the sediment should match the efflux of alkalinity across the sediment–water interface. The model predicts a total alkalinity production $R_\mathrm{sed} = 6.32\,\mathrm{mmol\,m^{-2}\,d^{-1}}$, which is indeed in good agreement with the mean A_T flux of 6.60 mmol $\mathrm{m^{-2}\,d^{-1}}$ as measured in our flux incubations within the SNS. Positive contributions to the A_T efflux are due to carbonate dissolution, aerobic respiration, denitrification, sulfate reduction and iron reduction, whereas A_T is consumed during nitrification, sulfur oxidation and pyrite formation. The most dominant A_T-producing reaction is carbonate dissolution, followed by sulfate reduction and denitrification. The most dominant A_T-consuming reactions are sulfide oxidation and nitrification. The A_T contribution of iron reduction is small and balances that of pyrite formation.

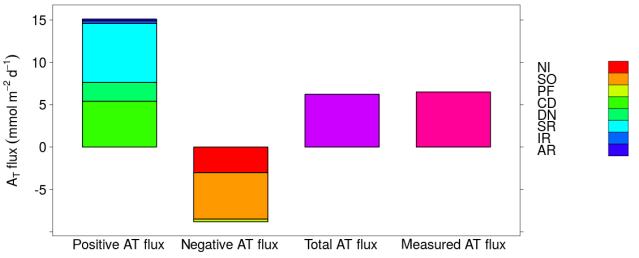

Figure 12. Contribution of different processes to the benthic A_T budget in the SNS. For more details on different reaction rates, see the text. NI: nitrification; SO: sulfide oxidation; PF: pyrite formation; CD: carbonate dissolution; DN: denitrification; SR: sulfate reduction; IR: dissimilatory iron reduction; AR: aerobic respiration. Fluxes in mmol m^{-2} d^{-1}.

4.5 System-wide alkalinity budget

Above we have documented how the sediments of the SNS can be a source of A_T for the water column of the SNS. However, before we can estimate the resulting effect of this benthic A_T release on the pCO_2 dynamics of the southern North Sea, we first need to assess the A_T balance of the water column. An efflux of A_T from the sediment does not necessarily result in an increase in A_T in the whole system, as in the water column, some biogeochemical processes oppose the A_T generation in the sediment. As noted above, the following calculations are based on measurements in June and September, and hence represent a budget for this period (not an annual average). Here, we identify carbonate formation (CF), primary production (PP), aerobic respiration (AR), and nitrogen fixation (NF) as processes that potentially produce or consume alkalinity in the water column.

As shown above, the dissolution of carbonates in the sediment (Eq. 4) forms a strong source of A_T, but the production of carbonates in the water column has the opposite effect on A_T.

$$Ca^{2+} + 2HCO_3^- \rightarrow CaCO_3 + CO_2 + H_2O \quad (13)$$

If the annual production of carbonate in the water column matches the carbonate dissolution in the sediments, there will be no net generation of A_T on a system-wide scale over a whole seasonal cycle. Note however that when there is a temporal shift in production versus dissolution of carbonates, these processes may still have an impact on the coastal A_T balance on shorter timescales. Here we assume that no net burial or export of solid carbonates occurs in the SNS on an annual scale (de Haas et al., 2002; Thomas et al., 2005; Bozec et al., 2006). Accordingly, the annual benthic carbonate dissolution must be fully compensated for by carbonate production in the water column; hence, carbonate production in the water column will consume 5.4 mmol m^{-2} d^{-1} of A_T.

A second process that consumes alkalinity in the water column is primary production. This is mostly pelagic, but also benthic in some very shallow waters of the SNS. If we assume that nitrate is the main nitrogen source, primary production can be described by the reaction equation

$$106CO_2 + 16NO_3^- + H_2PO_4^- + 122H_2O + 17H^+ \rightarrow OM + 138O_2. \quad (14)$$

Joint and Pomroy (1993) estimated primary production in the southern North Sea to be 199 g C m^{-2} yr^{-1}, or equally, 45.36 mmol C m^{-2} d^{-1}, thus producing 7.28 mmol m^{-2} d^{-1} of A_T. Note that Joint and Pomroy (1993) estimated annual primary production rate, whereas rates estimated in this study are based on summer measurements. In general, primary production rates are expected to be greater than the annual average in summer. Aerobic respiration in the water column can be described by the opposite reaction equation of primary production (Eq. 14). To estimate the total respiration rate, we need to account for two different sources of the organic matter that is being respired. The majority of the organic matter is derived from local primary production, while a smaller part originates from riverine input of terrestrial compounds. It has been estimated that about 80 % of the locally produced organic matter respires in the water column, whereas the remaining 20 % sinks down to the sediments (Radach and Moll, 1993; Moll, 1998). The value of $R_{min} = 10.3$ mmol m^{-2} d^{-1} as derived in the previous section, compares well with this assessment, as it comes down to 23 % of the PP value of 45.36 mmol C m^{-2} d^{-1} as estimated above. The pelagic mineralization rate derived from local net primary production hence becomes 35.06 mmol C m^{-2} d^{-1}. Additionally, organic matter input from land also fuels respiration, either in the water column or in the benthic compartment. The total riverine input of organic matter in the SNS was estimated by Kühn et al. (2010) to be in the range of 1.0 mmol C m^{-2} d^{-1}, which is hence small compared to the local net primary production. Accordingly, the total respiration rate in the water column must be 36.11 mmol C m^{-2} d^{-1}, thus consuming 5.79 mmol m^{-2} d^{-1} of A_T.

Finally, the loss of fixed nitrogen due to denitrification in the sediment can be compensated for by nitrogen fixation in the water column. However, the salinity of the North Sea is too high for diazotrophic cyanobacteria and too cold for open ocean cyanobacteria (Stal, 2009). Thus, we consider N_2 fixation in the North Sea to be negligible.

Similar to what was done for the sediment, we can define the total alkalinity generation in the water column R_{wc} as

$$R_{wc} = \frac{17}{106} r_{PP} - \frac{17}{106} r_{AR} - 2r_{CF} - r_{NF}, \quad (15)$$

which hence leads to a total consumption of 3.92 mmol m^{-2} d^{-1} of A_T.

Based on the analysis above, we can now write an alkalinity balance for the combined sediment and water column of the SNS:

$$\frac{\mathrm{d}}{\mathrm{d}t}\left[\int_0^{L_{\mathrm{sed}}} A_{\mathrm{T}}(z)\mathrm{d}z\right] = -F_{\mathrm{sed}} + R_{\mathrm{sed}}, \quad (16)$$

$$\frac{\mathrm{d}}{\mathrm{d}t}\left[\int_0^{L_{\mathrm{wc}}} A_{\mathrm{T}}(z)\mathrm{d}z\right] = F_{\mathrm{river}} + F_{\mathrm{sed}} - F_{\mathrm{out}} + R_{\mathrm{wc}}. \quad (17)$$

In summation of both mass balances, and assuming steady state, the alkalinity for the complete SNS system comprising both water column and sediment becomes

$$F_{\mathrm{river}} + F_{\mathrm{sed}} - R_{\mathrm{sed}} + R_{\mathrm{wc}} = 0. \quad (18)$$

This balance shows input and export processes (F terms) as well as processes that cause internal alkalinity generation (R terms). The total net generation of alkalinity in the SNS amounts to $R_{\mathrm{net}} = R_{\mathrm{sed}} + R_{\mathrm{wc}} = 6.32 - 3.92 = 2.40\,\mathrm{mmol\,m^{-2}\,d^{-1}}$ or $244\,\mathrm{Gmol\,yr^{-1}}$. Furthermore, the riverine input of alkalinity was estimated by Pätsch and Kühn (2008) as $F_{\mathrm{river}} = 1.5\,\mathrm{mmol\,m^{-2}\,d^{-1}}$, based on a river load compilation for the years 1977 to 2002. Accordingly, the A_{T} export flux from the SNS to the rest of the North Sea (SKNT and NNS) is $F_{\mathrm{out}} = F_{\mathrm{river}} + R_{\mathrm{sed}} + R_{\mathrm{wc}} = 1.5 + 6.32 - 3.92 = 3.90\,\mathrm{mmol\,m^{-2}\,d^{-1}}$ or $398\,\mathrm{Gmol\,yr^{-1}}$. Additionally, A_{T} from the Wadden Sea might increase the A_{T} budget of the SNS. Schwichtenberg (2013) estimated that $\approx 68\,\%$ of the yearly A_{T} change in the German Bight is due to A_{T} export from the Wadden Sea. Thomas et al. (2009) estimated an A_{T} flux from the Wadden Sea into the SNS of $9.6\,\mathrm{mmol\,m^{-2}\,d^{-1}}$. However, the important question is whether the Wadden Sea exports "uncompensated" TA that then drives CO_2 uptake in the SNS. Any net A_{T} generation in the Wadden Sea will generally also induce an atmospheric CO_2 uptake in that area. If the residence time of the water is sufficiently long, water masses of the Wadden Sea will be in equilibrium with respect to CO_2 in the atmosphere. In this scenario, the net A_{T} generation in the Wadden Sea will be fully compensated for by CO_2 uptake in the Wadden Sea, and so this will not influence the air–sea CO_2 exchange of the SNS. In the absence of reliable estimates, uncompensated A_{T} inputs from the Wadden Sea were ignored in the budget here, and so the F_{river} terms for DIC and TA must be interpreted as inputs from both rivers and the Wadden Sea to the SNS.

As shown in Table 5, the different terms that contribute to net generation of alkalinity in the SNS have been attributed to four different types of elemental cycling (carbon, nitrogen, sulfur + iron, phosphate). This analysis reveals that no alkalinity is associated with carbon and phosphate cycling, but that 26 % can be attributed to sulfur and iron cycling (i.e., anoxic mineralization taking place in the sediment), and the remaining 74 % is linked to nitrogen cycling (this part is dominated by denitrification in the sediment). Sedimentary denitrification is hence the most prominent driver of net alkalinity generation in the SNS. Applying our estimated mean denitrification rate ($1.9\,\mathrm{mmol\,N\,m^{-2}\,d^{-1}}$) to the whole SNS, this implies a removal of $194\,\mathrm{Gmol\,N\,yr^{-1}}$ of bioavailable nitrogen, which is roughly twice as high as the denitrification estimate of Pätsch and Kühn (2008) of $119\,\mathrm{Gmol\,N\,yr^{-1}}$ for the whole North Sea. However, whereas our estimation covers mainly the summer months, Pätsch and Kühn (2008) calculated an annual average rate. Accounting for the fact that the sediments of the SNS are the prime locations for denitrification, our estimates of denitrification rates and the associated alkalinity generation rate in the SNS seem to be in line with previous studies.

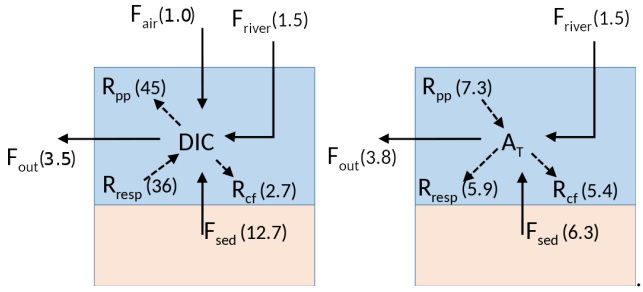

Figure 13. DIC and A_{T} budgets of the water column in the SNS. Bold arrows: fluxes; dashed arrows: reaction rates. F_{sed}: net flux from the sediments; F_{river}: riverine input; F_{out}: flux into the NNS/SKNT; F_{air}: atmospheric DIC uptake; R_{pp}: primary production rate; R_{resp}: aerobic respiration rate; R_{cf}: carbonate production rate. Unit: $\mathrm{mmol\,C\,m^{-2}\,d^{-1}}$

4.6 Impact on water column pCO_2 dynamics of the SNS

Figure 13 shows the associated DIC and A_{T} budget of the water column in the SNS. The direction of a CO_2 flux between the surface water and the atmosphere is determined by the pCO_2 gradient between water and atmosphere, which is ultimately governed by the ratio of internal DIC over internal A_{T} release (Frankignoulle, 1994; Egleston et al., 2010; Hu and Cai, 2011b). As shown above, the net generation of alkalinity amounts to $2.40\,\mathrm{mmol\,m^{-2}\,d^{-1}}$. Similarly the net generation of DIC amounts to $1.0\,\mathrm{mmol\,m^{-2}\,d^{-1}}$. As we assume that organic matter burial is negligible, there is no net internal net DIC generation due to respiration of locally produced organic matter (the respiration of autochtonous organic matter in both water column and sediment matches the primary production of autochtonous organic matter in the water column). However, as noted above, riverine input of organic matter, and so respiration of this organic matter, releases $1.0\,\mathrm{mmol\,C\,m^{-2}\,d^{-1}}$ of DIC. At constant atmospheric CO_2 and retaining a constant alkalinity, one can calculate that the addition of 1 mole A_{T} to seawater will lead to an addition of 0.85 mole of DIC. This calculation

was carried out in R using the AquaEnv package, utilizing the values of Millero et al. (2006) for the first and second dissociation constants of carbonic acid in seawater (Hofmann et al., 2010), and assuming mean parameters of the SNS for the time of sampling (salinity: 34 PSU; temperature: 16.3 °C; A_T: 2270 µmol kg^{-1}) and an atmospheric CO_2 concentration of 392 ppm). Accordingly, a net internal alkalinity release of 2.40 mmol m^{-2} d^{-1} will hence lead to an associated DIC increase of 1.96 mmol C m^{-2} d^{-1}. Of this, 1.0 mmol C m^{-2} d^{-1} is already supplied by internal DIC generation, and so, the remainder of 0.96 mmol m^{-2} d^{-1} will be supplied by CO_2 uptake from the atmosphere. The CO_2 uptake for the SNS as a whole amounts to 98 Gmol C yr^{-1}, which is around 14 % of the total CO_2 uptake of the entire North Sea (Thomas et al., 2004; Egleston et al., 2010). This value is slightly lower than the estimate by Thomas et al. (2009), who calculated that sedimentary A_T can potentially facilitate up to 25 % of the total CO_2 uptake of the North Sea. This latter estimate was not based on direct flux measurements, but was derived from an A_T budget for the North Sea, where A_T generation in Wadden Sea sediments was introduced as a closure term.

The idea that internal alkalinity generation in the SNS can drive atmospheric CO_2 uptake is further supported by previous CO_2 studies, although significant seasonality has been observed in the atmospheric CO_2 uptake. Thomas et al. (2005) reported an uptake of CO_2 for the months of February to August (-0.52 mmol C m^{-2} d^{-1}), while the SNS was reported to be a source of CO_2 between September and January ($+0.60$ mmol C m^{-2} d^{-1}). Bozec et al. (2005) described the SNS as a strong source of CO_2 with fluxes of 0.8 to 1.7 mmol C m^{-2} d^{-1} in late summer, while on an annual scale, the SNS was characterized as a sink of CO_2 with an air–sea flux of -0.55 mmol C m^{-2} d^{-1}. Due to the temporal variability of CO_2 fluxes, and the seasonal cycles of primary production and respiration, it is hard to compare these numbers with our calculated CO_2 air–sea flux based on internal A_T generation only, but the estimated impact on the pCO_2 dynamics of the SNS by benthic A_T release appears to be on the same order of magnitude as determined in previous studies of the pCO_2 dynamics of the SNS. Overall, the A_T release from sediments, driven by denitrification and anoxic respiration of organic matter, seems to play an important role in the atmospheric CO_2 uptake of the North Sea.

Acknowledgements. We thank W.-J. Cai and J. Paetsch for their reviews, which greatly improved the manuscript. Furthermore, the excellent cooperation of the captain and the crew of R/V *Pelagia* is gratefully acknowledged. We are further indebted to Marco Houtekamer, Jurian Brasser and Jan Peene for help with the sampling processing as well as to Alexandra Rao for providing training and advice prior to the cruises. We also thank Will Burt for providing us with the data of Fig. 10 and further input regarding sediment–water exchange rates. This paper has benefited significantly from fruitful discussions with Mathilde Hagens. This work was supported by the ZKO program of the Netherlands Organisation for Scientific Research (NWO) and supported by the European Research Council under the European Union's Seventh Framework Programme (FP/2007-2013) through ERC grant 306933 to F. J. R. Meysman. U. Braeckman was financially supported by FWO project no. G.0033.11.

Edited by: G. Herndl

References

Archer, D. and Devol, A.: Benthic oxygen fluxes on the Washington shelf and slope: A comparison of in situ microelectrode and chamber flux measurements, Limnol. Oceanogr., 37, 614–629, 1992.

Bauer, J. E., Cai, W.-J., Raymond, P. A., Bianchi, T. S., Hopkinson, C. S., and Regnier, P. A.: The changing carbon cycle of the coastal ocean, Nature, 504, 61–70, 2013.

Berelson, W., McManus, J., Coale, K., Johnson, K., Burdige, D., Kilgore, T., Colodner, D., Chavez, F., Kudela, R., and Boucher, J.: A time series of benthic flux measurements from Monterey Bay, CA, Cont. Shelf Res., 23, 457–481, 2003.

Berner, R. A. and Westrich, J. T.: Bioturbation and the early diagenesis of carbon and sulfur, Am. J. Sci., 285, doi:10.2475/ajs.285.3.193, 1985.

Boetius, A. and Damm, E.: Benthic oxygen uptake, hydrolytic potentials and microbial biomass at the Arctic continental slope, Deep-Sea Res. Pt. I, 45, 239–275, 1998.

Boon, A., Duineveld, G., Berghuis, E., and Van der Weele, J.: Relationships between benthic activity and the annual phytopigment cycle in near-bottom water and sediments in the southern North Sea, Estuar. Coast. Shelf S., 46, 1–13, 1998.

Borges, A. V. and Frankignoulle, M.: Distribution of surface carbon dioxide and air-sea exchange in the English Channel and adjacent areas, J. Geophys. Res.-Oceans, 108, 2156–2209, 2003.

Boudreau, B. P., Middelburg, J. J., Hofmann, A. F., and Meysman, F. J.: Ongoing transients in carbonate compensation, Global Biogeochem. Cy., 24, GB4010, doi:10.1029/2009GB003654, 2010.

Bozec, Y., Thomas, H., Elkalay, K., and de Baar, H. J.: The continental shelf pump for CO_2 in the North Sea-evidence from summer observation, Mar. Chem., 93, 131–147, 2005.

Bozec, Y., Thomas, H., Schiettecatte, L.-S., Borges, A. V., Elkalay, K., and De Baar, H. J.: Assessment of the processes controlling the seasonal variations of dissolved inorganic carbon in the North Sea, Limnol. Oceanogr., 51, 2746–2762, 2006.

Braeckman, U., Foshtomi, M. Y., Van Gansbeke, D., Meysman, F., Soetaert, K., Vincx, M., and Vanaverbeke, J.: Variable importance of macrofaunal functional biodiversity for biogeochemical cycling in temperate coastal sediments, Ecosystems, 17, 720–737, 2014.

Brasse, S., Reimer, A., Seifert, R., and Michaelis, W.: The influence of intertidal mudflats on the dissolved inorganic carbon and total alkalinity distribution in the German Bight, southeastern North Sea, J. Sea Res., 42, 93–103, doi:10.1016/S1385-1101(99)00020-9, 1999.

Burt, W., Thomas, H., Pätsch, J., Omar, A., Schrum, C., Daewel, U., Brenner, H., and Baar, H.: Radium isotopes as a tracer of

sediment-water column exchange in the North Sea, Global Biogeochem. Cy., 28, 786–804, 2014.
Cai, W.-J. and Sayles, F. L.: Oxygen penetration depths and fluxes in marine sediments, Mar. Chem., 52, 123–131, 1996.
Cai, W.-J., Dai, M., and Wang, Y.: Air-sea exchange of carbon dioxide in ocean margins: A province-based synthesis, Geophys. Res. Lett., 33, doi:10.1029/2006GL026219, 2006.
Chen, C.-T. A.: Shelf-vs. dissolution-generated alkalinity above the chemical lysocline, Deep-Sea Res. Part II, 49, 5365–5375, 2002.
Chen, C.-T. A. and Borges, A. V.: Reconciling opposing views on carbon cycling in the coastal ocean: Continental shelves as sinks and near-shore ecosystems as sources of atmospheric CO_2, Deep-Sea Res. Pt. II, 56, 578–590, 2009.
Chen, C.-T. A. and Wang, S.-L.: Carbon, alkalinity and nutrient budgets on the East China Sea continental shelf, J. Geophys. Res.-Oceans, 104, 20675–20686, 1999.
Cramer, A.: Seasonal variation in benthic metabolic activity in a frontal system in the North Sea, Trophic relationships, 54–76, 1990.
Dauwe, B.: Organic matter quality in North Sea sediments, PhD thesis, Rijksuniversiteit Groningen, Groningen, 1999.
de Haas, H. and van Weering, T. C.: Recent sediment accumulation, organic carbon burial and transport in the northeastern North Sea, Mar. Geol., 136, 173–187, 1997.
de Haas, H., van Weering, T. C., and de Stigter, H.: Organic carbon in shelf seas: sinks or sources, processes and products, Cont. Shelf Res., 22, 691–717, 2002.
DelValls, T. and Dickson, A.: The pH of buffers based on 2-amino-2-hydroxymethyl-1, 3-propanediol ("tris") in synthetic sea water, Deep-Sea Res. Pt. I, 45, 1541–1554, 1998.
Denman, K. and Pena, M.: The response of two coupled one-dimensional mixed layer/planktonic ecosystem models to climate change in the NE subarctic Pacific Ocean, Deep-Sea Res. Pt. II, 49, 5739–5757, 2002.
Devol, A. H. and Christensen, J. P.: Benthic fluxes and nitrogen cycling in sediments of the continental margin of the eastern North Pacific, J. Mar. Res., 51, 345–372, 1993.
Dickson, A. G., Sabine, C. L., Christian, J. R.: Guide to best practices for ocean CO_2 measurements, no. 3 in PICES Special Publication, North Pacific Marine Science Organization, Sidney, British Columbia, 2007.
Egleston, E. S., Sabine, C. L., and Morel, F. M.: Revelle revisited: Buffer factors that quantify the response of ocean chemistry to changes in DIC and alkalinity, Global Biogeochem. Cy., 24, GB1002, doi:10.1029/2008GB003407, 2010.
Elliott, A., Clarke, T., and Li, Z.: Monthly distributions of surface and bottom temperatures in the northwest European shelf seas, Cont. Shelf Res., 11, 453–466, 1991.
Fennel, K.: The role of continental shelves in nitrogen and carbon cycling: Northwestern North Atlantic case study, Ocean Sci., 6, 539–548, doi:10.5194/os-6-539-2010, 2010.
Franco, M. d. A., Vanaverbeke, J., Van Oevelen, D., Soetaert, K., Costa, M. J., Vincx, M., and Moens, T.: Respiration partitioning in contrasting subtidal sediments: seasonality and response to a spring phytoplankton deposition, Mar. Ecol., 31, 276–290, 2010.
Frankignoulle, M.: A complete set of buffer factors for acid/base CO_2 system in seawater, J. Marine Syst., 5, 111–118, 1994.
Frankignoulle, M., Abril, G., Borges, A., Bourge, I., Canon, C., Delille, B., Libert, E., and Théate, J.-M.: Carbon dioxide emission from European estuaries, Science, 282, 434–436, 1998.
Friedl, G., Dinkel, C., and Wehrli, B.: Benthic fluxes of nutrients in the northwestern Black Sea, Mar. Chem., 62, 77–88, 1998.
Gattuso, J.-P., Frankignoulle, M., and Wollast, R.: Carbon and carbonate metabolism in coastal aquatic ecosystems, Annual Review of Ecology and Systematics, 29, 405–434, 1998.
Glud, R. N.: Oxygen dynamics of marine sediments, Mar. Biol. Res., 4, 243–289, 2008.
Grasshoff, K., Kremling, K., and Ehrhardt, M.: Methods of seawater analysis, John Wiley & Sons, Hoboken, New Jersey, 2009.
Grebmeier, J. M. and McRoy, C. P.: Pelagic-benthic coupling on the shelf of the northern Bering and Chukchi Seas. 111. Benthic food supply and carbon cycling, Mar. Ecol.-Prog. Ser., 53, 79–91, 1989.
Gustafsson, B. and Stigebrandt, A.: Dynamics of the freshwater-influenced surface layers in the Skagerrak, J. Sea Res., 35, 39–53, 1996.
Gustafsson, E., Wällstedt, T., Humborg, C., Mörth, C.-M., and Gustafsson, B. G.: External total alkalinity loads versus internal generation: The influence of nonriverine alkalinity sources in the Baltic Sea, Global Biogeochem. Cy., 28, 1358–1370, 2014.
Hartnett, H., Boehme, S., Thomas, C., DeMaster, D., and Smith, C.: Benthic oxygen fluxes and denitrification rates from high-resolution porewater profiles from the Western Antarctic Peninsula continental shelf, Deep-Sea Res. Pt. II, 55, 2415–2424, 2008.
Hebbeln, D., Scheurle, C., and Lamy, F.: Depositional history of the Helgoland mud area, German Bight, North Sea, Geo-Mar. Lett., 23, 81–90, 2003.
Hofmann, A. F., Soetaert, K., Middelburg, J. J., and Meysman, F. J. R.: AquaEnv : An Aquatic Acid-Base Modelling Environment in R, Aquat. Geochem., 16, 507–546, 2010.
Hu, X. and Cai, W.-J.: An assessment of ocean margin anaerobic processes on oceanic alkalinity budget, Global Biogeochem. Cy., 25, GB3003, doi:10.1029/2010GB003859, 2011a.
Hu, X. and Cai, W.-J.: The impact of denitrification on the atmospheric CO_2 uptake potential of seawater, Mar. Chem., 127, 192–198, 2011b.
Huettel, M. and Gust, G.: Solute release mechanisms from confined sediment cores in stirred benthic chambers and flume flows, Mar. Ecol.-Prog. Ser., 82, 187–197, 1992.
Huettel, M. and Rusch, A.: Transport and degradation of phytoplankton in permeable sediment, Limnol. Oceanogr., 45, 534–549, 2000.
Hydes, D., Kelly-Gerreyn, B., Le Gall, A., and Proctor, R.: The balance of supply of nutrients and demands of biological production and denitrification in a temperate latitude shelf sea – a treatment of the southern North Sea as an extended estuary, Mar. Chem., 68, 117–131, 1999.
Jahnke, R. A. and Jahnke, D. B.: Calcium carbonate dissolution in deep sea sediments: reconciling microelectrode, pore water and benthic flux chamber results, Geochim. Cosmochim. Ac., 68, 47–59, 2004.
Jahnke, R. A., Craven, D. B., and Gaillard, J.-F.: The influence of organic matter diagenesis on CaCO 3 dissolution at the deep-sea floor, Geochim. Cosmochim. Ac., 58, 2799–2809, 1994.

Janssen, F., Faerber, P., Huettel, M., Meyer, V., and Witte, U.: Pore-water advection and solute fluxes in permeable marine sediments(I): Calibration and performance of the novel benthic chamber system Sandy, Limnol. Oceanogr., 50, 768–778, 2005.

Joint, I. and Pomroy, A.: Phytoplankton biomass and production in the southern North Sea, North East Atlantic Marine Research Programme, Great Britain, 1993.

Jönsson, B. F., Salisbury, J. E., and Mahadevan, A.: Large variability in continental shelf production of phytoplankton carbon revealed by satellite, Biogeosciences, 8, 1213–1223, doi:10.5194/bg-8-1213-2011, 2011.

Jørgensen, B. B.: The sulfur cycle of a coastal marine sediment (Limfjorden, Denmark) , Limnol. Oceanogr., 22, 814–832, 1977.

Jørgensen, B. B., Bang, M., and Blackburn, T. H.: Anaerobic mineralization in marine-sediments from the Baltic-Sea-North-Sea transition, Mar. Ecol.-Prog. Ser., 59, 39–54, 1990.

Kitidis, V., Hardman-Mountford, N. J., Litt, E., Brown, I., Cummings, D., Hartman, S., Hydes, D., Fishwick, J. R., Harris, C., Martinez-Vicente, V., and Woodward, E. M. S.: Seasonal dynamics of the carbonate system in the Western English Channel, Cont. Shelf Res., 42, 30–40, 2012.

Krumins, V., Gehlen, M., Arndt, S., Van Cappellen, P., and Regnier, P.: Dissolved inorganic carbon and alkalinity fluxes from coastal marine sediments: model estimates for different shelf environments and sensitivity to global change, Biogeosciences, 10, 371–398, doi:10.5194/bg-10-371-2013, 2013.

Kühn, W., Pätsch, J., Thomas, H., Borges, A. V., Schiettecatte, L.-S., Bozec, Y., and Prowe, A. F.: Nitrogen and carbon cycling in the North Sea and exchange with the North Atlantic – A model study, Part II: Carbon budget and fluxes, Cont. Shelf Res., 30, 1701–1716, 2010.

Lansard, B., Rabouille, C., Denis, L., and Grenz, C.: In situ oxygen uptake rates by coastal sediments under the influence of the Rhône River (NW Mediterranean Sea), Cont. Shelf Res., 28, 1501–1510, 2008.

Larsen, M., Thamdrup, B., Shimmield, T., and Glud, R. N.: Benthic mineralization and solute exchange on a Celtic Sea sand-bank (Jones Bank), Prog. Oceanogr., 117, 64–75, 2013.

Lehrter, J. C., Beddick, D. L., Devereux, R., Yates, D. F., and Murrell, M. C.: Sediment-water fluxes of dissolved inorganic carbon, O2, nutrients, and N2 from the hypoxic region of the Louisiana continental shelf, Biogeochemistry, 109, 233–252, 2011.

Lenhart, H. and Pohlmann, T.: The ICES-boxes approach in relation to results of a North Sea circulation model, Tellus A, 49, 139–160, 1997.

Lohse, L., Malschaert, J. F. P., Slomp, C. P., Helder, W., and van Raaphorst, W.: Nitrogen cycling in North Sea sediments: interaction of denitrification and nitrification in offshore and coastal areas, Mar. Ecol.-Prog. Ser., 101, 283–283, 1993.

Lohse, L., Kloosterhuis, H. T., Van Raaphorst, W., and Helder, W.: Denitrification rates as measured by the isotope pairing method and by the acetylene inhibition technique in continental shelf sediments of the North Sea, Marine ecology progress series, Oldendorf, 132, 169–179, 1996.

Lüders, K.: Sediments of the North Sea, Special Publications of SEPM, Wilhelmshaven, Germany, 1955.

Luff, R. and Moll, A.: Seasonal dynamics of the North Sea sediments using a three-dimensional coupled sediment-water model system, Cont. Shelf Res., 24, 1099–1127, 2004.

Meysman, F. J. R., Galaktionov, O. S., Cook, P. L. M., Janssen, F., Huettel, M., and Middelburg, J. J.: Quantifying biologically and physically induced flow and tracer dynamics in permeable sediments, Biogeosciences, 4, 627–646, doi:10.5194/bg-4-627-2007, 2007.

Middelburg, J. J., Soetaert, K., Herman, P. M., and Heip, C. H.: Denitrification in marine sediments: A model study, Global Biogeochem. Cy., 10, 661–673, 1996.

Millero, F. J., Graham, T. B., Huang, F., Bustos-Serrano, H., and Pierrot, D.: Dissociation constants of carbonic acid in seawater as a function of salinity and temperature, Mar. Chem., 100, 80–94, 2006.

Moll, A.: Regional distribution of primary production in the North Sea simulated by a three-dimensional model, J. Marine Syst., 16, 151–170, 1998.

Moore, W., Beck, M., Riedel, T., van der Loeff, M. R., Dellwig, O., Shaw, T. J., Schnetger, B., and Brumsack, H.-J.: Radium-based pore water fluxes of silica, alkalinity, manganese, DOC, and uranium: A decade of studies in the German Wadden Sea, Geochim. Cosmochim. Ac., 75, 6535–6555, 2011.

Nedwell, D., Parkes, R., Upton, A., and Assinder, D.: Seasonal fluxes across the sediment-water interface, and processes within sediments, Philos. T. R. S.-A., 343, 519–529, 1993.

Nordi, G., Debes, H., and Christensen, J. T.: Pelagic-benthic coupling on the Faroe shelf: a pilot study, Tech. rep., Faroe Marine Research Institute, Tórshavn, Faroe Island, 2013.

Osinga, R., Kop, A. J., Duineveld, G. C. A., Prins, R. A., Duyl, F. C. V., and Fleur, C.: Benthic mineralization rates at two locations in the southern North Sea, J. Sea Res., 36, 181–191, 1996.

Pätsch, J. and Kühn, W.: Nitrogen and carbon cycling in the North Sea and exchange with the North Atlantic – a model study. Part I. Nitrogen budget and fluxes, Cont. Shelf Res., 28, 767–787, 2008.

Paulmier, A., Kriest, I., and Oschlies, A.: Stoichiometries of remineralisation and denitrification in global biogeochemical ocean models, Biogeosciences, 6, 923–935, doi:10.5194/bg-6-923-2009, 2009.

Provoost, P., Heuven, S. V., Soetaert, K., Laane, R. W. P. M., Middelburg, J. J., and van Heuven, S.: Seasonal and long-term changes in pH in the Dutch coastal zone, Biogeosciences, 7, 3869–3878, doi:10.5194/bg-7-3869-2010, 2010.

Provoost, P., Braeckman, U., Van Gansbeke, D., Moodley, L., Soetaert, K., Middelburg, J. J., and Vanaverbeke, J.: Modelling benthic oxygen consumption and benthic-pelagic coupling at a shallow station in the southern North Sea, Estuar. Coast. Shelf S., 120, 1–11, 2013.

Radach, G. and Moll, A.: Estimation of the variability of production by simulating annual cycles of phytoplankton in the central North Sea, Prog. Oceanogr., 31, 339–419, 1993.

Rao, A. M., Polerecky, L., Ionescu, D., Meysman, F. J. R., and De Beer, D.: The influence of pore-water advection, benthic photosynthesis, and respiration on calcium carbonate dynamics in reef sands, Limnol. Oceanogr., 57, 809–825, 2012.

Rao, A. M., Malkin, S. Y., Montserrat, F., and Meysman, F. J.: Alkalinity production in intertidal sands intensified by lugworm bioirrigation, Estuar. Coast. Shelf S., 148, 36–47, 2014.

Redfield, A. C.: The biological control of chemical factors in the environment, Am. Sci., 46, 230A–221, 1958.

Regnier, P., Friedlingstein, P., Ciais, P., Mackenzie, F. T., Gruber, N., Janssens, I. A., Laruelle, G. G., Lauerwald, R., Luyssaert, S.,

Andersson, A. J., and Arndt, S.: Anthropogenic perturbation of the carbon fluxes from land to ocean, Nat. Geosci., 6, 597–607, 2013.

Reid, P. C. and Edwards, M.: Long-term changes in the pelagos, benthos and fisheries of the North Sea, Senck. Marit., 31, 107–115, 2001.

Richards, F.: Anoxic basins and Fjords In Chemical Oceanography, 611–643, edited by: Richards, F. A., Ripley, J. P., and Skirrow, G., 1965.

Rodhe, J.: The large-scale circulation in the Skagerrak; interpretation of some observations, Tellus A, 39, 245–253, 1987.

Rodhe, J.: On the dynamics of the large-scale circulation of the Skagerrak, J. Sea Res., 35, 9–21, 1996.

Santschi, P. H., Anderson, R. F., Fleisher, M. Q., and Bowles, W.: Measurements of diffusive sublayer thicknesses in the ocean by alabaster dissolution, and their implications for the measurements of benthic fluxes, J. Geophys. Res.-Oceans, 96, 10641–10657, 1991.

Schiettecatte, L.-S., Thomas, H., Bozec, Y., and Borges, A.: High temporal coverage of carbon dioxide measurements in the Southern Bight of the North Sea, Mar. Chem., 106, 161–173, 2007.

Schlüter, M. and Jerosch, K.: Digital Atlas of the North Sea, Alfred Wegener Institute for Polar and Marine Research, Bremerhaven, Germany, 2009.

Schrum, C., Alekseeva, I., and John, M. S.: Development of a coupled physical–biological ecosystem model ECOSMO: part I: model description and validation for the North Sea, J. Marine Syst., 61, 79–99, 2006.

Schwichtenberg, F.: Drivers of the carbonate system variability in the southern North Sea: River input, anaerobic alkalinity generation in the Wadden Sea and internal processes, PhD thesis, Fakultät für Mathematik, Informatik und Naturwissenschaften im Fachbereich Geowissenschaften der Universität Hamburg, 2013.

Seitzinger, S., Harrison, J. A., Böhlke, J., Bouwman, A., Lowrance, R., Peterson, B., Tobias, C., and Drecht, G. V.: Denitrification across landscapes and waterscapes: a synthesis, Ecol. Appl., 16, 2064–2090, 2006.

Shum, K.: Wave-induced advective transport below a rippled water-sediment interface, J. Geophys. Res.-Oceans, 97, 789–808, 1992.

Slomp, C., Malschaert, J., Lohse, L., and Van Raaphorst, W.: Iron and manganese cycling in different sedimentary environments on the North Sea continental margin, Cont. Shelf Res., 17, 1083–1117, 1997.

Smith Jr., K.: Oxygen demands of San Diego Trough sediments: an in situ study, Limnol. Oceanogr, 19, 939–944, 1974.

Soetaert, K., Petzoldt, T., and Meysman, F. J. R.: marelac: Tools for Aquatic Sciences, NIOO-KNAW, Yerseke, the Netherlands, 2010.

Stal, L. J.: Is the distribution of nitrogen-fixing cyanobacteria in the oceans related to temperature?, Environ. Microbiol., 11, 1632–1645, 2009.

Tengberg, A., Hall, P. O. J., Andersson, U., Lindén, B., Styrenius, O., Boland, G., de Bovee, F., Carlsson, B., Ceradini, S., Devol, A., and Duineveld, G.: Intercalibration of benthic flux chambers, Mar. Chem., 1, 147–173, 2005.

Thamdrup, B. and Canfield, D. E.: Benthic respiration in aquatic sediments, in: Methods in ecosystem science, Springer, New York, 86–103, 2000.

Thamdrup, B., Fossing, H., and Jørgensen, B. B.: Manganese, iron and sulfur cycling in a coastal marine sediment, Aarhus Bay, Denmark, Geochim. Cosmochim. Ac., 58, 5115–5129, 1994.

Therkildsen, M. S. and Lomstein, B. A.: Seasonal variation in net benthic C-mineralization in a shallow estuary, FEMS Microbiol. Ecol., 12, 131–142, 1993.

Thomas, H., Bozec, Y., Elkalay, K., and de Baar, H. J. W.: Enhanced open ocean storage of CO2 from shelf sea pumping, Science, 304, 1005–1008, 2004.

Thomas, H., Bozec, Y., de Baar, H. J. W., Elkalay, K., Frankignoulle, M., Schiettecatte, L.-S., Kattner, G., and Borges, A. V.: The carbon budget of the North Sea, Biogeosciences, 2, 87–96, doi:10.5194/bg-2-87-2005, 2005.

Thomas, H., Schiettecatte, L.-S., Suykens, K., Koné, Y. J. M., Shadwick, E. H., Prowe, A. E. F., Bozec, Y., de Baar, H. J. W., and Borges, A. V.: Enhanced ocean carbon storage from anaerobic alkalinity generation in coastal sediments, Biogeosciences, 6, 267–274, doi:10.5194/bg-6-267-2009, 2009.

Trimmer, M., Nedwell, D., Sivyer, D., and Malcolm, S.: Seasonal benthic organic matter mineralisation measured by oxygen uptake and denitrification along a transect of the inner and outer River Thames estuary, UK, Mar. Ecol.-Prog. Ser., 197, 103–119, 2000.

Trimmer, M., Petersen, J., Sivyer, D., Mills, C., Young, E., and Parker, E.: Impact of long-term benthic trawl disturbance on sediment sorting and biogeochemistry in the southern North Sea, Mar. Ecol.-Prog. Ser., 298, 79–94, 2005.

Upton, A.: Seasonal benthic microbial activity in the southern North Sea; oxygen uptake and sulphate reduction, Mar. Ecol.-Prog. Ser., 101, 273–281, 1993.

Van der Molen, J.: The influence of tides, wind and waves on the net sand transport in the North Sea, Con. Shelf Res., 22, 2739–2762, 2002.

Van Duyl, F. C., Bak, R. P., Kop, A. J., Nieuwland, G., Berghuis, E. M., and Kok, A.: Mesocosm experiments: mimicking seasonal developments of microbial variables in North Sea sediments, Hydrobiologia, 235, 267–281, 1992.

Van Raaphorst, W., Kloosterhuis, H. T., Cramer, A., and Bakker, K. J.: Nutrient early diagenesis in the sandy sediments of the Dogger Bank area, North Sea: Pore water results, Neth. J. Sea Res., 26, 25–52, 1990.

Weston, K., Fernand, L., Nicholls, J., Marca-Bell, A., Mills, D., Sivyer, D., and Trimmer, M.: Sedimentary and water column processes in the Oyster Grounds: a potentially hypoxic region of the North Sea, Mar. Environ. Res., 65, 235–249, 2008.

Wilde, P., Berghuis, E., and Kok, A.: Structure and energy demand of the benthic community of the Oyster Ground, central North Sea, Neth. J. Sea Res., 18, 143–159, doi:10.1016/0077-7579(84)90029-2, 1984.

Witte, U. and Pfannkuche, O.: High rates of benthic carbon remineralisation in the abyssal Arabian Sea, Deep-Sea Res. Pt. II, 47, 2785–2804, 2000.